Effect of Membrane Potential on Entry of Lactoferricin B-Derived 6-Residue Antimicrobial Peptide into Single Escherichia coli Cells and Lipid Vesicles

Effect of membrane potential on entry of lactoferricin B-derived 6-residue antimicrobial peptide into single *Escherichia coli* cells and lipid vesicles

Farzana Hossain[1], Hideo Dohra[2], and Masahito Yamazaki[1,3,4,*]

From the [1]Integrated Bioscience Section, Graduate School of Science and Technology, [2]Instrumental Research Support Office, Research Institute of Green Science and Technology, [3]Nanomaterials Research Division, Research Institute of Electronics, [4]Department of Physics, Graduate School of Science, Shizuoka University, Shizuoka 422-8529, Japan

Running title: Membrane potential affects antimicrobial peptide entry

*To whom correspondence should be addressed: Masahito Yamazaki, Nanomaterials Research Division, Research Institute of Electronics, Shizuoka University, 836 Oya, Suruga-ku, Shizuoka 422-8529, Japan; yamazaki.masahito@shizuoka.ac.jp, Tel/Fax: 81-(54)-238-4741

Key words: antimicrobial peptides, membrane biophysics, *Escherichia coli*, lipid vesicle, lipid bilayer, peptide entry, giant unilamellar vesicle, spheroplast, leakage, membrane potential

ABSTRACT

The antimicrobial peptide (AMP) derived from lactoferricin B, LfcinB (4-9) (RRWQWR), and lissamine rhodamine B red-labeled peptide (Rh-LfcinB (4-9)) exhibit strong antimicrobial activities, and they can enter *Escherichia coli* cells without damaging the cell membranes. Thus, these peptides are cell-penetrating peptide (CPP) -type AMPs. In this study, to elucidate the effect of the membrane potential ($\Delta\varphi$) on the action of the CPP-type AMP, Rh-LfcinB (4-9), we investigated the interactions of Rh-LfcinB (4-9) with single *E. coli* cells and spheroplasts containing calcein in the cytosol using confocal laser scanning microscopy. At low peptide concentrations, Rh-LfcinB (4-9) entered the cytosol of single *E. coli* cells and spheroplasts without damaging the cell membranes, and the H^+-ionophore carbonyl cyanide *m*-chlorophenyl-hydrazone (CCCP) suppressed its entry. The studies using the time-kill method indicate that these low concentrations of peptide exhibit antimicrobial activity but CCCP inhibits this activity. Next, we investigated the effect of $\Delta\varphi$ on the interaction of Rh-LfcinB (4-9) with single giant unilamellar vesicles (GUVs) comprising *E. coli* polar lipid extracts and containing a fluorescent probe, Alexa Fluor 647 hydrazide. At low concentrations (0.2–0.5 μM), Rh-LfcinB (4-9) showed significant entry to the single GUV lumen without pore formation in the presence of $\Delta\varphi$. The fraction of entry of peptide increased with increasing negative membrane potential, indicating that the rate of peptide entry into the GUV lumen increased with increasing negative membrane potential. These results indicate that $\Delta\varphi$ enhances the entry of Rh-LfcinB (4-9) into single *E. coli* cells, spheroplasts, and GUVs and its antimicrobial activity.

IMPORTANCE

Bacterial cells have a membrane potential ($\Delta\varphi$), but the effect of $\Delta\varphi$ on action of cell-penetrating peptide-type antimicrobial peptides (AMPs) is not clear. Here, we investigated the effect of $\Delta\varphi$ on the action of fluorescent probe-labeled AMP derived from lactoferricin B, Rh-LfcinB (4-9). At low peptide concentrations, Rh-LfcinB (4-9) enters the cytosol of *Escherichia coli* cells and spheroplasts without damaging their cell membrane, but a protonophore suppresses this entry and its antimicrobial activity. The rate of entry of Rh-LfcinB (4-9) into the giant unilamellar vesicles (GUVs) comprising *E. coli* lipids without pore formation increases with increasing $\Delta\varphi$. These results indicate that $\Delta\varphi$ enhances the antimicrobial activity of Rh-LfcinB (4-9) and hence LfcinB (4-9) by increasing the rate of their entry into the cytosol.

Introduction

Antimicrobial peptides (AMPs) have bacteriostatic or bactericidal activity. AMPs typically target the bacterial cell membrane, damaging the membrane and inducing significant membrane permeation of the internal cell contents (1-6). For example, some AMPs such as LL-37 and lactoferricin B (LfcinB) were observed to enhance membrane permeation from live bacterial cells (7,8). On the other hand, some AMPs, such as buforin II (9) and a short fragment of LfcinB, LfcinB (4-9) (10), can enter the cytosol of bacterial cells without significant leakage. These AMPs have a similar activity of translocation across cell membranes to cell-penetrating peptides (CPPs), and hence are categorized as CPP-type AMPs. The terms “CPP-type AMPs” and “AMPs with CPP properties” have a wide range of meanings and several definitions (11,12). One of the definitions of CPP-type AMPs is that these AMPs enter the cytosol of eukaryotic cells in a similar manner to CPPs (e.g., Bac7(1-35) and LL-37 (13,14)). Another definition is that these AMPs must bind to a

specific protein in the cytoplasm to elicit its bactericidal effect; thus, all D amino acid analogues lack antimicrobial activity (e.g., apidaecin and pyrrhocoricin (15,16)). It is proposed that apidaecin enters the cytosol by sequential molecular interactions (15). In this report, we use the term "CPP-type AMPs" in the narrow sense that AMPs that enter the cytosol by translocating across the lipid bilayer region of the plasma membrane without damaging the membrane, subsequently bind to DNA and/or cytosolic proteins. Hence, the main target of the bactericidal effect of CPP-type AMPs is not the cell membrane, but DNA and/or proteins in the cytoplasm of bacterial cells (17). Therefore, translocation across the cell membrane to enter the cytosol is an essential step of their antimicrobial activity.

Live bacterial cells have a large negative membrane potential, and it has been suggested that the membrane potential ($\Delta\varphi$) affects the action of AMPs (18,19). The change in $\Delta\varphi$ affects the location of membrane proteins, making it difficult to elucidate which process of the AMP-induced damage of cell membranes is affected by changes in membrane potential (20-23). Recently, we reported that the rate constant of AMP-induced damage to lipid bilayers (i.e., lactoferricin B-induced local rupture of a lipid bilayer and magainin 2-induced pore formation in a lipid bilayer) increased with increasing negative membrane potential of giant unilamellar vesicles (GUVs) (8,24). These GUVs do not contain membrane proteins or other proteins that interact with the membrane, clearly indicating that the membrane potential greatly affects the interaction of AMPs with lipid bilayers and the AMP-induced damage of the lipid bilayers. On the other hand, we also found that the rate of entry of another type of peptide, a CPP known as transportan 10 (TP10), into the lumen of single GUVs increased with increasing negative membrane potential (25). However, data on the effect of $\Delta\varphi$ on the action of AMPs remains limited (26). Especially, there has been no study on the effect of $\Delta\varphi$ on the action of CPP-type AMPs.

In the present study, we investigated the effect of $\Delta\varphi$ on the action of one of the CPP-type AMPs, LfcinB (4-9), using single *E. coli* cells, spheroplasts, and GUVs. LfcinB (4-9) (RRWQWR) exhibits the highest antimicrobial activity among several AMPs obtained by the hydrolysis of lactoferricin B (27,28). The fluorescent probe, lissamine rhodamine B red-labeled LfcinB (4-9) (i.e., Rh-LfcinB (4-9)) also exhibits high antimicrobial activity, because the minimum inhibitory concentration (MIC) of Rh-LfcinB (4-9) and LfcinB (4-9) are 5 μM and 25 μM, respectively (10). It has been reported that Rh-LfcinB (4-9) can enter the cytosol of *E. coli* cells as well as single GUVs composed of negatively charged dioleoylphosphatidylglycerol (DOPG) and electrically neutral dioleoylphosphatidylcholine (DOPC) mixtures (1/1; molar ratio) (i.e., DOPG/DOPC (1/1)-GUVs) without leakage of the internal contents of the GUV lumen (10). These results indicate that the behavior of Rh-LfcinB (4-9) is similar to that of CPPs. In the present study, we first examined the interaction of Rh-LfcinB (4-9) with single *E. coli* cells to reveal the mode of entry of this peptide into their cytoplasm. For this purpose, we investigated the interaction of Rh-LfcinB (4-9) with live single *E. coli* cells containing calcein in the cytosol using confocal laser scanning microscopy (CLSM). Further, we assessed the effect of the protonophore (i.e., H^+-ionophore), carbonyl cyanide *m*-chloro-phenylhydrazone (CCCP), which can induce the dissipation of $\Delta\varphi$ in *E. coli* cells (22), on this interaction. We also examined the effect of CCCP on Rh-LfcinB (4-9)-induced decrease in cell viability using the time-kill method. Next, we examined the interaction of Rh-LfcinB (4-9) with single spheroplasts derived from *E. coli* cells to reveal its direct interaction with the cell membrane as well as the effect of CCCP on this interaction. Finally, we examined the effect of $\Delta\varphi$ on Rh-LfcinB (4-9) entry into single GUVs composed of *E. coli* polar lipid extract (*E. coli*-lipid) using the single GUV method for CPPs (25, 29). Based on these results, we discuss the effect of

$\Delta\varphi$ on the mode of entry of Rh-LfcinB (4-9) into the cytoplasm of cells and its translocation across the cell membrane and the lipid bilayer.

Results

Effect of membrane potential on Rh-LfcinB (4-9) entry into single E. coli cells

Recently, we demonstrated that Rh-LfcinB (4-9) enters the cytosol of single *E. coli* cells without leakage of calcein, i.e., without damage to cell membranes (10). However, in that study, the interaction of Rh-LfcinB (4-9) with single *E. coli* cells was examined in a buffer, where the cells were in a starvation condition (30-33). Here, we investigated the interaction of Rh-LfcinB (4-9) with single *E. coli* cells in an EZ rich medium, where the cells are actively growing (8, 34). The water-soluble fluorescent probe calcein was loaded to the cytosol of *E. coli* cells by using the interaction between calcein-AM and *E. coli* cells (8, 35).

First, we examined the interaction of 5.0 μM Rh-LfcinB (4-9) with single *E. coli* cells in an EZ rich medium in a microchamber at 25 °C using CLSM. The peptide solution (in EZ rich medium) was continuously provided to the vicinity of a cell through a micropipette. Figure 1A shows the result for non-septating cells. During the peptide interaction, the fluorescence intensity (FI) of the *E. coli* cell due to calcein decreased gradually (up to 10 min) (Fig. 1A (1) and the green line in Fig. 1C). The mean decrease in normalized FI after 10 min was 26 ± 3 % (n = 19). On the other hand, we observed a similar gradual decrease in FI in single cells without peptide interaction (Fig. S1 in the Supporting Information) and the mean decrease in normalized FI after 10 min was 29 ± 3 % (n = 21). The gradual decrease in FI and the mean values of the decrease in normalized FI after 10 min observation are almost the same in the presence and absence of peptide interaction. Thus, we can reasonably infer that this gradual decrease in FI observed in Fig. 1a is due to the

photobleaching of calcein. In contrast, the FI of the total cell due to Rh-LfcinB (4-9) increased somewhat with time to reach a steady value at ~35 s, which remained almost constant for 120 s, and then gradually increased from 153 s to reach a high value (Fig. 1A (2) and the red line in Fig. 1C). Figure 1B shows the FI profiles along the white line in the image in Fig. 1A (0 s of the calcein image). Initially (at less than 153 s), the FI due to Rh-LfcinB (4-9) at the rim of the cell corresponding to the membrane (i.e., the rim intensity) was greater than the FI at the central region of the cell corresponding to the cytosol; however, after 153 s the FI at the central region became greater than the rim intensity. The initial weak intensity at the rim is attributed to the binding of Rh-LfcinB (4-9) to the membrane, and the gradual, large increase in FI from 153 s is due to peptide entry into the cytosol. As the criterion for peptide entry into the cytosol, here we used the condition that the FI at the central region of a cell is larger than the rim intensity.

The same experiments were performed using 13 *E. coli* cells (i.e., 9 non-septating and 4 septating cells) (n = 13). We found that the entry of Rh-LfcinB (4-9) into the cytosol occurred without great decrease in FI due to calcein in 8 cells (i.e., 5 non-septating and 3 septating cells). In Fig. 1D, each curve corresponds to the time course of FI due to Rh-LfcinB (4-9) for each cell during the interaction of 5.0 μM peptide, indicating a wide distribution of rates of peptide entry into the cytosol of a single cell. The rate of entry in septating cells was greater than that in non-septating cells (see the curves labeled by “S” in Fig. 1D for the time course of the septating cells and the nonlabeled curves for that of non-septating cells). These results indicate that Rh-LfcinB (4-9) outside the *E. coli* cell entered its cytosol without pore formation in the cell membrane. In contrast, for other *E. coli* cells, the FI of the central region of the cells did not become greater than the rim intensity of the cells within 10 min. The FI of the total cell was also low (Fig. 1D). This suggests that Rh-LfcinB (4-9) outside the cell could not enter the cytosol. Under this condition,

the entry of the peptide into its cytosol was observed in 62% of total examined cells. As a measure of the rate of entry of Rh-LfcinB (4-9) into the cytosol of the *E. coli* cells, we can use the fraction of cells in which Rh-LfcinB (4-9) entered before a specific time t without pore formation with respect to the total number of examined cells (hereafter, fraction of entry), $P_{entry}(t)$. The above results indicate that P_{entry} (10 min) is 0.62. The mean value and SD of P_{entry} (10 min) was 0.64 ± 0.03 (2 independent experiments (i.e., $N = 2$) using 12 – 13 cells each time).

We next examined the effect of peptide concentration on the entry of Rh-LfcinB (4-9) into single cells without leakage of calcein. At a peptide concentration of 9.0 μM, peptide entry into the cytosol was observed in all examined cells (i.e., $n = 12$; 8 non-septating and 4 septating cells); thus, P_{entry} (10 min) = 1.0. In some cells, the FI of *E. coli* cells due to calcein decreased greatly, indicating the leakage of calcein (Fig. S2 (A) (B) in Supporting Information) and pore formation in the cell membrane. Prior to beginning leaking, the FI of cells due to Rh-LfcinB (4-9) increased, indicating that Rh-LfcinB (4-9) entered the cell before pore formation. However, after leakage, the FI due to the peptide greatly increased. This suggests that the peptides entered the cytosol through pores or damaged sites in the cell membrane. On the other hand, in other cells, Rh-LfcinB (4-9) entry occurred but leakage of calcein was not observed by 10 min (Fig. S2 (C) (D)). At a peptide concentration of 2.0 μM, P_{entry} (10 min) was 0.46 ± 0.05, but the FI of the total cell due to Rh-LfcinB (4-9) was low at 10 min (Fig. S3). In contrast, at 1.0 μM peptide, among the examined cells (i.e., 12 cells; 9 non-septating cells and 3 septating cells), the FI of the cytosol was lower than that of the rim in 9 cells (8 non-septating and 1 septating cells), indicating that in most cells the peptide could not enter the cytosol. Figure 1E shows the peptide concentration dependence of P_{entry} (10 min), indicating that the cell-penetrating activity of Rh-LfcinB (4-9) against *E. coli* increased in a concentration-dependent manner. Figure 1E also shows the peptide concentration dependence

of the fraction of leaked cells among all examined cells at 10 min, P_{leak} (10 min). At a peptide concentration of 5.0 μM and less, no leakage occurred in all cells (i.e., P_{leak} (10 min) = 0); in contrast, at 9.0 μM peptide, P_{leak} (10 min) = 0.38 ± 0.06.

The results of Fig.1 indicate that at low peptide concentrations (2.0 and 5.0 μM) Rh-LfcinB (4-9) enters *E. coli* cells significantly without damage of plasma membranes. It is important to check the effect of these low concentrations of peptides on the cell viability or growth of cells, because in the case of higher peptide concentration (9.0 μM) it is difficult to identify the cause of inhibition of cell growth and cell death clearly (i.e., there are two possible causes: the entry of peptide into the cytosol and the damage of the plasma membrane). We reported previously that the MIC of Rh-LfcinB (4-9) against the same strain of *E. coli* cells is 5.0 μM (10). Thus, it is clear that 5.0 μM peptide exhibited the inhibition of growth of cells. We also used the time-kill method (36) to elucidate the antimicrobial activity of these low concentrations of Rh-LfcinB (4-9). In this method, the time course of the fraction of viable cells in an *E. coli* cell suspension in the presence of AMPs is estimated by measuring the number of live cells (colony forming unit (CFU)/mL) using the agar plate count method. Figure 2 shows that the fraction of live cells in an *E. coli* cell suspension containing 5.0 μM peptide decreased with time, and 99.9% reduction was achieved after 3 h. The fraction of live cells in an *E. coli* cell suspension containing 2.0 μM peptide decreased gradually with time up to 4 h. These results indicate that these low concentrations of Rh-LfcinB (4-9) have antimicrobial activity without damage of plasma membranes.

Next, we investigated the effect of the H^+-ionophore CCCP on the entry of Rh-LfcinB (4-9) into single *E. coli* cells to elucidate the role of membrane potential in peptide entry. It is well known that CCCP decreases $\Delta\varphi$ (22). In the presence of 100 μM CCCP in EZ rich medium (final concentration), we investigated the interaction of 5.0 μM Rh-LfcinB (4-9) with single *E. coli* cells

at 25 °C. A gradual decrease in FI due to calcein occurred during the interaction (up to 10 min) (Fig. 3A, B) due to the photobleaching of calcein, indicating that the peptide did not induce any damage to the cell membrane through which calcein leaked. On the other hand, the increase in FI due to Rh-LfcinB (4-9) was small (Fig. 3A, B). This result indicates that while the peptide bound with the cell membrane, it could not enter the cytosol, P_{entry} (10 min) = 0 and P_{leak} (10 min) = 0 (N = 2 each using 10-12 cells). Therefore, we can conclude that $\Delta\varphi$ plays an important role in the entry of Rh-LfcinB (4-9) into the cytosol of *E. coli* cells.

To investigate the effect of CCCP on the antimicrobial activity of Rh-LfcinB (4-9) against *E. coli* cells, we applied the time-kill method to examine the Rh-LfcinB (4-9)-induced decrease in cell viability in the presence and absence of CCCP. After the interaction of 5.0 μM Rh-LfcinB (4-9) with *E. coli* cells in the presence and absence of 100 μM CCCP for 15 min at 25 °C, we diluted 100−1000 times with the medium to remove CCCP and the peptides from the cells, and then measured the number of live cells (CFU/mL) using the agar plate count method and obtained the fraction of viable cells in an *E. coli* cell suspension. As shown in Table 1, the fraction of viable cells interacting with 5.0 μM peptide in the presence of 100 μM CCCP was 0.71 ± 0.04, which is much larger than that in the absence of CCCP (0.24 ± 0.05). The former value is similar to the fraction of viable cells in the presence of 100 μM CCCP only (i.e., no peptides) (0.77 ± 0.03), indicating that for the former case the main cause to decrease the cell viability is the presence of CCCP. These results show that the presence of CCCP greatly diminished the antimicrobial activity of Rh-LfcinB (4-9) whereas CCCP in itself decreased cell viability a little. It is well known that CCCP decreases $\Delta\varphi$ (22), and thus, we can conclude that the antimicrobial activity of Rh-LfcinB (4-9) is large in the presence of negative membrane potential.

Interaction of Rh-LfcinB (4-9) with single E. coli spheroplasts

E. coli cells have a complicated cell envelope, comprising an outer membrane, a peptidoglycan layer and a cell membrane. In the interaction of AMPs with these cells, there may be many targets for AMPs. Thus, it is generally considered that the interpretation of the experimental results on the interaction of AMPs with cells is not straightforward. In contrast, *E. coli* spheroplasts have only cell membranes, allowing us to obtain information on the direct interaction of AMPs with the cell membrane (8,37). In this section, we examined the interaction of Rh-LfcinB (4-9) with single *E. coli* spheroplasts containing calcein in the cytosol using CLSM.

During 10 min observation of a single spheroplast containing calcein in the absence of peptide, the FI of the inside of the spheroplast decreased (Fig. S4 in Supporting Information), which is attributed to the photobleaching of calcein. The mean decrease in normalized FI of the spheroplast after 10 min was 30 ± 6% (n = 6), which is the same as that observed in *E. coli* cells within experimental errors. We have previously reported similar photobleaching (8), where LfcinB induced rapid leakage of calcein from single spheroplasts and thus some photobleaching did not affect the interpretation of the results. However, in this report, to decrease photobleaching, the FI of a spheroplast interacting with peptide was observed for 20–30 s (sometime 60 s) at intervals of ~200 s or ~50 s; otherwise the shutter of the incident laser was closed.

First, we investigated the interaction of 2.0 μM Rh-LfcinB (4-9) with single spheroplasts in spheroplast buffer. Figure 4A shows that FI due to calcein did not decrease significantly (Fig. 4A (1) and green circles in Fig. 4B). During the interaction of the Rh-LfcinB (4-9) solution with the spheroplast, the FI of the spheroplast membrane (i.e., the rim intensity) due to Rh-LfcinB (4-9) initially increased to reach a small, steady value (800) at 100 s, which was kept constant for ~400 s. After 480 s, it increased a little. Figure 4C shows the FI profile along the white line in the image

of Fig. 4A (2) (0 s of Rh-LfcinB (4-9) image). The FI of the rim of the spheroplast is greater than the FI of its central region, indicating that this FI is due to the binding of Rh-LfcinB (4-9) to the cell membrane of the spheroplast. The FI of the spheroplast rim remained constant from 100 to 480 s, indicating that the peptide concentration in the membrane is constant. During this time, the FI of its central region due to Rh-LfcinB (4-9) increased with time (Fig. 4C and red line in Fig. 4B). These results indicate that Rh-LfcinB (4-9) entered the cytosol of spheroplasts. The experiment shown in Fig. 4A was repeated using 10 single spheroplasts, and similar results were obtained. Rh-LfcinB (4-9) entered the cytosol of 5 spheroplasts. Thus, the fraction of entry into spheroplast cytosol, P_{entry} (10 min) is 0.50. We performed two independent same experiments as above (N = 2), and obtained P_{entry} (10 min) = 0.52 ± 0.04.

Next, we examined the interaction of 3.0 μM Rh-LfcinB (4-9) with single spheroplasts under the same conditions (Fig. 5A). The FI due to calcein did not decrease significantly in the beginning but decreased greatly after 260 s (Fig. 5B), indicating the occurrence of calcein leakage. The FI of its central region of the spheroplast due to Rh-LfcinB (4-9) gradually increased with time, and after 260 s it increased rapidly (Fig. 5B). The rim intensity of spheroplasts due to Rh-LfcinB (4-9) increased with time (Fig. 5B). Figure 5C shows the FI profiles along the white line in the image in Fig. 5A (2) (0 s of the Rh-LfcinB (4-9) image). Initially (at less than 200 s), the rim intensity was greater than the FI at the central region of the cell corresponding to the cytosol; however, after 260 s the FI at the central region became greater than the rim intensity. These results indicate that that Rh-LfcinB (4-9) entered the cytosol of spheroplasts prior to pore formation. Following pore formation, the rate of peptide entry increased. Among 12 spheroplasts, we observed the entry of Rh-LfcinB (4-9) before calcein leakage in 11 spheroplasts and the leakage of calcein in 7 spheroplasts. We obtained a mean P_{entry} (10 min) value of 0.86 ± 0.09 (N = 2). Figure 4D shows

that P_{entry} (10 min) increased with increasing peptide concentration. On the other hand, Fig. 5D shows the peptide concentration dependence of the fraction of leaked spheroplasts among all examined spheroplasts at 10 min, P_{leak} (10 min). At 2.0 μM peptide, no leakage occurred in all spheroplasts (i.e., P_{leak} (10 min) = 0), while at 3.0 μM peptide, P_{leak} (10 min) = 0.65 ± 0.07.

It is reported that *E. coli* spheroplasts have a membrane potential (38). We examined the effect of CCCP on the interaction of Rh-LfcinB (4-9) with single spheroplasts to elucidate the role of $\Delta\varphi$ on peptide entry. First, in the presence of 100 μM CCCP in the spheroplast buffer, we examined the interaction of 5.0 μM Rh-LfcinB (4-9) with single spheroplasts at 25 °C. A gradual decrease in FI due to calcein occurred during the interaction (up to 10 min) (Fig. 6A, B), attributed to calcein photobleaching. This result indicates that Rh-LfcinB (4-9) did not induce any damage to the cell membrane resulting in calcein leakage. On the other hand, the increase in FI attributed to Rh-LfcinB (4-9) was minimal. This result suggests that Rh-LfcinB (4-9) bound with the cell membrane but did not enter the cytosol. The same experiments were performed using many spheroplasts, and similar results were observed, i.e., $P_{leak} = 0$ and $P_{entry} = 0$ ($N = 2$ each using 10-12 spheroplasts). These results indicate that $\Delta\varphi$ in spheroplasts plays an important role in Rh-LfcinB (4-9) entry to the cytosol of spheroplasts.

Effect of membrane potential on entry of Rh-LfcinB (4-9) into single E. coli-lipid-GUVs

To elucidate the mechanism of the effect of $\Delta\varphi$ on Rh-LfcinB (4-9) entry into the cytosol of *E. coli* cells and spheroplasts, we investigated the entry of Rh-LfcinB (4-9) into the lumen of single GUVs composed of *E. coli* polar lipid extract (*E. coli*-lipid) (phosphatidylethanolamine (PE) / phosphatidylglycerol (PG) / cardiolipin (CA) = 67/23/10 (wt% ratio)), which has a similar lipid composition to the *E. coli* cell membrane. To assess Rh-LfcinB (4-9) entry into the GUV lumen

and pore formation in the membrane, we employed the single GUV method for CPPs (25,29). In this method, single GUVs (i.e., mother GUVs) containing small GUVs 1−10 μm in diameter and a water-soluble fluorescent probe, AF647, in the lumen were used (25,29). During the interaction of fluorescent probe-labeled CPPs with single GUVs, the detection of fluorescence due to CPPs at small GUVs in the mother GUV lumen indicates the entry of CPPs into the lumen.

First, we investigated the interaction of 5.0 μM Rh-LfcinB (4-9) with single *E. coli*-lipid GUVs in the absence of $\Delta\varphi$. During the peptide interaction, FI in the GUV lumen due to AF647 remained constant over 10 min (Fig. 7A (1) and 7B), indicating that leakage of AF 647 did not occur during the interaction, i.e., no pore formation in the mother GUV membrane. Figures 7A (2) and 7B show that the rim intensity due to Rh-LfcinB (4-9) rapidly increased to a maximum at 15 s, then decreased somewhat, and finally reached a steady value at 100 s, indicating that the peptide concentration in the GUV membrane increased to reach a steady value. This decrease in rim intensity may be due to quenching of rhodamine fluorescence due to a high concentration of Rh-LfcinB (4-9) in the GUV membrane. On the other hand, there was no fluorescence in the mother GUV lumen at the beginning of the interaction, whereas beginning at 106 s, we detected fluorescence at the small GUVs in the GUV lumen without leakage of AF647 (Fig. 7A (2)). These results indicate that Rh-LfcinB (4-9) entered the GUV lumen and bound to the small GUVs without pore formation (25,29). Among the 16 examined GUVs, we detected the entry of peptides in 9 GUVs; thus, P_{entry} (10 min) = 0.56. Two independent experiments each using 10-16 GUVs provided P_{entry} (10 min) = 0.53 ± 0.04. We did not observe leakage of AF647 after 10 min reaction, i.e., P_{leak} (10 min) = 0.

We also examined the effect of peptide concentration on the entry of Rh-LfcinB (4-9) into GUVs without pore formation. Figure 7C shows the Rh-LfcinB (4-9) concentration dependence of P_{entry} (10 min). At peptide concentrations of ≤ 0.5 μM, a significant entry of Rh-LfcinB (4-9) into

GUVs was not observed during 10 min interaction. At a concentration of 2.0 μM and greater, entry of Rh-LfcinB (4-9) was observed in some examined GUVs, and P_{entry} (10 min) increased with an increase in peptide concentration. At 9.0 μM Rh-LfcinB (4-9), P_{entry} (10 min) was 0.76 ± 0.13. We did not observe AF647 leakage after 10 min reaction for all peptide concentrations ≤ 9.0 μM, i.e., P_{leak} (10 min) = 0. Moreover, the rim intensity depended on peptide concentration. In the interaction of 0.5 μM Rh-LfcinB (4-9) with a single GUV, the rim intensity gradually increased with time, and its steady value is smaller than that of 5.0 μM Rh-LfcinB (4-9) (Fig. 7D).

Next, we examined the effect of $\Delta\varphi$ on the entry of Rh-LfcinB (4-9) into single *E. coli*-lipid-GUVs. Membrane potentials were applied only to the mother *E. coli*-lipid-GUV membranes containing gramicidin A (gA) using various K^+ concentration differences between the GUV lumen and its outside. First, we investigated the effect of $\Delta\varphi$ on the entry of 0.50 μM Rh-LfcinB (4-9) into single GUVs, since in the absence of $\Delta\varphi$ significant peptide entry into GUVs was not detected during 10 min interaction (Fig. 7C). Figure 8A (1) shows a typical result for the interaction of 0.50 μM Rh-LfcinB (4-9) with *E. coli*-lipid-GUVs at $\Delta\varphi = -102$ mV. The FI in the GUV lumen due to AF647 remained essentially constant over the 10 min interaction (Fig. 8A (1) and 8C). This result shows that AF 647 did not leak during the interaction, indicating that no pores were formed in the mother GUV membrane. Figures 8A (2) and 8C show that the rim intensity due to Rh-LfcinB (4-9) rapidly increased to a maximum at 60 s, then decreased somewhat, and finally reached a steady value at 100 s. This decrease in rim intensity may be due to quenching of rhodamine fluorescence due to a high concentration of Rh-LfcinB (4-9) in the GUV membrane. In contrast, at the beginning, fluorescence was not detected in the GUV lumen, but at 239 s and later we observed fluorescent small GUVs in the mother GUV lumen (Fig. 8A (2)). These results indicate that Rh-LfcinB (4-9) enters the GUV lumen and binds to small GUVs without pore formation. Among the 12 examined

GUVs, we observed peptide entry in 11 GUVs, P_{entry} (10 min) = 0.92. Two independent experiments each using 8-12 GUVs provided P_{entry} (10 min) = 0.90 ± 0.03.

As a control experiment, we investigated the interaction of Rh-LfcinB (4-9) with single GUVs of the same lipid composition (i.e., *E. coli*-lipid and gA mixture) at $\Delta\varphi = 0$ mV. Under this condition, P_{entry} (10 min) = 0.05 ± 0.07 (Fig. 8B). The rim intensity due to Rh-LfcinB (4-9) gradually increased to reach a steady value at 200 s, which was smaller than that at $\Delta\varphi = -102$ mV (Fig. 8D). A transient decrease in rim intensity due to quenching was not observed at $\Delta\varphi = 0$ mV. For $\Delta\varphi = -59$ mV, P_{entry} (10 min) = 0.39 ± 0.02 (n = 18). These results indicate that P_{entry} (10 min) increased as the negative membrane potential increased (Fig. 8E). We did not observe the leakage of AF647 after 10 min reaction for all peptide concentrations at the membrane potential examined here.

We also examined the effect of $\Delta\varphi$ on the entry of different concentrations (2.0 and 0.20 μM) of Rh-LfcinB (4-9), and a similar result was obtained. Figure 8E shows that irrespective of peptide concentration, the fraction of Rh-LfcinB (4-9) entry increased as the negative membrane potential increased, indicating that the rate of peptide entry was elevated with the increase in negative membrane potential.

Discussion

In this study, we demonstrated the effect of $\Delta\varphi$ on the entry of Rh-LfcinB (4-9) into the cytosol of *E. coli* cells and their spheroplasts, as well as the lumen of *E. coli* lipid-GUVs. First, at low concentrations (≤ 5.0 μM) Rh-LfcinB (4-9) enters the cytosol of single *E. coli* cells without damaging the cell membrane, and the proton-ionophore CCCP suppresses this entry. Moreover, the presence of CCCP inhibits the antimicrobial activity of Rh-LfcinB (4-9) against *E. coli* cells These results demonstrate the correlation between the antimicrobial activity and the efficiency (or

the rate) of entry of this peptide into the cytosol. Second, at low concentrations (≤ 2.0 μM) Rh-LfcinB (4-9) enters the cytosol of single *E. coli* spheroplasts without damaging the cell membrane, and CCCP suppresses this entry. Third, lower concentrations (0.2–0.5 μM) of Rh-LfcinB (4-9) significantly enter the single GUV lumen without pore formation in the presence of membrane potential. The fraction of entry of Rh-LfcinB (4-9) increases with increasing negative membrane potential, indicating that the rate of peptide entry into the single GUV lumen increases with increasing negative membrane potential. These results indicate that the membrane potential enhances the rate of the entry of Rh-LfcinB (4-9) into single GUVs and *E. coli* cells. It is reported that nonlabeled LfcinB (4-9) and Rh-LfcinB (4-9) bind strongly with DNA (10), which may induce bacterial cell death (17). For CPP-type AMPs, the increase in the rate of peptide entry into cytoplasm is one of the main causes of their enhanced antimicrobial activity. Therefore, the results in this study indicate that the antimicrobial activity of Rh-LfcinB (4-9) increases with negative membrane potential.

In this study, to reveal the correlation between the entry of Rh-LfcinB (4-9) and peptide-induced pore formation, we simultaneously measured the time courses of the entry of peptide (into the cytosol of *E. coli* cells and their spheroplasts, and the lumen of *E. coli* lipid-GUVs) and the leakage of internal contents such as calcein and AF647. Based on these measurements, we succeeded in detecting and discriminating peptide entry without pore formation and the entry through pores in the membrane. For example, we consider the results of the interaction of Rh-LfcinB (4-9) with single spheroplasts and GUVs. At low concentrations of Rh-LfcinB (4-9), the peptide enters the cytosol of *E. coli* spheroplasts without pore formation. At Rh-LfcinB (4-9) concentrations greater than 3.0 μM, peptide entry into the cytosol occurs first and leakage of calcein occurs subsequently in some spheroplasts ($P_{leak} = 0.65 \pm 0.07$), indicating that Rh-LfcinB

(4-9) induces pore formation in the cell membrane. After pore formation, the peptide concentration in the cytosol greatly increases, which is likely to be due to peptide entry through pores. In contrast, in the interaction of Rh-LfcinB (4-9) with *E. coli*-lipid-GUVs, the peptide enters the GUV lumen without leakage of AF647 for reactions up to 10 min at all peptide concentrations ≤ 9.0 μM. This result indicates that the interaction of Rh-LfcinB (4-9) with the lipid bilayer regions of the cell membrane of spheroplasts does not induce the formation of pores through which calcein leaks. Therefore, comparison of the results of spheroplasts and GUVs suggests that in the case of spheroplasts, after Rh-LfcinB (4-9) enters the cytosol, it binds with resident proteins or DNA that induce pore formation in the cell membrane. On the other hand, in the interaction of Rh-LfcinB (4-9) with *E. coli* cells, leakage of calcein did not occur after 10 min reaction for all peptide concentrations of ≤ 5.0 μM, whereas a peptide concentration of 9.0 μM induced leakage. The difference between *E. coli* cells and spheroplasts may suggest that Rh-LfcinB (4-9) binds the outer membrane and/or peptidoglycans of *E. coli* and thus the effective Rh-LfcinB (4-9) concentration near the cell membrane in the cells decreases.

Moreover, we observed the rapid entry of Rh-LfcinB (4-9) into the cytosol of *E. coli* cells and their spheroplasts at less than 10 min; thus, it is reasonable to suggest that peptide entry is the initial step in the cell death mechanism. In most studies of AMPs, researchers examined the location of peptides using fluorescence microscopy and electron microscopy at specific longer durations (e.g., 30 min and 2 h) of peptide interaction with bacterial cells. Since the plasma membrane becomes leaky after cell death, peptides can easily enter the cytosol through the damaged membrane. In this case, peptide entry can be considered as an effect of cell death, rather than the cause of cell death. If the time course of peptide entry is not measured, we cannot determine whether peptide entry into the cytosol is the cause or the result of cell death.

In the interaction of Rh-LfcinB (4-9) with *E. coli* cells and their spheroplasts, it is necessary to consider many factors such as membrane proteins, proteins which can interact with the cell membrane, and DNA. Suppression of membrane potential due to CCCP also induces many changes such as the location of proteins. Therefore, elucidating the effect of membrane potential on the interaction of the peptide with the lipid bilayer region of cell membranes is challenging. In contrast, examining the interaction of Rh-LfcinB (4-9) with *E. coli*-lipid-GUVs enables consideration of the interaction of the peptide with the pure lipid bilayer alone, as well as the effect of $\Delta\varphi$ on this interaction. The fraction of Rh-LfcinB (4-9) entry into *E. coli*-lipid-GUVs at 10 min interaction, P_{entry} (10 min), which is a measure of the rate of entry of Rh-LfcinB (4-9), greatly increased with increasing negative membrane potential. For example, for 0.50 μM Rh-LfcinB (4-9) P_{entry} (10 min) increased from 0.05 at $\Delta\varphi = 0$ mV to 0.39 at −59 mV, then to 0.90 at −102 mV. This result clearly demonstrates that membrane potential enhances the rate of entry of Rh-LfcinB (4-9) to single GUVs. This membrane potential dependence is somewhat smaller than that of the fraction of entry of CF-TP10 into DOPG/DOPC-GUVs (for example, for 0.5 μM CF-TP10 P_{entry} (6 min) increased from 0 at $\Delta\varphi = 0$ mV to 1.0 at − 59 mV) (25).

Here, we consider the mechanism underlying the effect of $\Delta\varphi$ on Rh-LfcinB (4-9) entry. The rim intensity results of single GUVs exposed to Rh-LfcinB (4-9) indicate that the steady, maximum concentration of peptides in the GUV membrane, as well as the rate of increase of peptide concentration in the GUV membrane, increase with increasing membrane potential (Fig. 8D). However, the quenching of Rh fluorescence at a higher membrane potential prevents the accurate estimation of the $\Delta\varphi$ dependence of peptide concentration in the GUV membrane. In the case of interaction of various concentrations of Rh-LfcinB (4-9) with single GUVs at $\Delta\varphi = 0$ mV, we observed a similar phenomenon: the steady, maximum concentration of peptides in the GUV

membrane increases with peptide concentration in aqueous solution, although at higher concentrations, the quenching of Rh fluorescence occurs (Fig. 7D). This result supports the interpretation on the effect of $\Delta\varphi$ on the rim intensity. In our previous report, we investigated the effect of membrane potential on the entry of the CPP TP10 into the single GUV lumen (25). The rate of entry of CF-TP10 and the rim intensity due to CF-TP10 (which is proportional to the CF-TP10 concentration in the GUV membrane) increased with an increase in negative membrane potential. It is known that CF-TP10 translocates across the lipid bilayer from the outer leaflet to the inner leaflet. Based on these results, we inferred that the increase in CF-TP10 concentration in the inner leaflet is the main cause of the increase in the rate of entry of CF-TP10 into the GUV lumen with increasing negative membrane potential (25). This result can be explained by a decrease in the electrostatic interaction energy between the positive charges of CF-TP10 and the electric potential inside the membrane due to the negative membrane potential. Based on the results of this study, we can infer that the increase in the rate of Rh-LfcinB (4-9) entry with negative membrane potential is induced by the increase in peptide concentration in the GUV membrane with increasing negative membrane potential.

It is generally considered that the fluorescent labeling of peptides and proteins may affect their function and interactions with membranes. However, in the effect of membrane potential on AMPs (24) and CPPs (25), the interaction of the positive charges of these peptides with the electric potential inside the membrane due to the negative membrane potential plays an important role. The Rh moiety does not have a charge; thus, one can reasonably infer that the attachment of Rh to LfcinB (4-9) does not impact the effect of membrane potential on peptide entry into the cytoplasm. Therefore, the results in this study suggest that membrane potential increases the rate of entry of nonlabeled LfcinB (4-9) into the cytoplasm, thus increasing its antimicrobial activity.

For the pathway of the entry of CPPs into the cytoplasm of eukaryotic cells, endocytosis and direct permeation through the plasma membrane have been considered (39,40). However, in most bacterial cells including *E. coli* cells, there is no endocytosis system (41). Thus, we can reasonably infer that the entry of Rh-LfcinB (4-9) into the cytosol of *E. coli* cells occurs through direct permeation through the plasma membrane. Several mechanisms for the translocation of peptides such as CPPs across the lipid bilayer have been proposed (42). One is the pore model: first peptides induce a pore in the lipid bilayer, through which peptides permeate to translocate across the lipid bilayer (43-45). The pore is defined as a water channel, which opens for an extended time and through which small water-soluble fluorescent probes such as calcein and AF647 can permeate. In the case of the interaction of Rh-LfcinB (4-9) with *E. coli*-lipid-GUVs and DOPG/DOPC-GUVs (10), such pores are not produced, and thus, this pore model cannot explain the translocation of Rh-LfcinB (4-9). Another model is the inverted micelle model: positively charged peptides form a complex with a specific amount of negatively-charged lipids, and the resulting structure of the complex is similar to an inverted micelle (46-48). We recently proposed a new model referred to as the prepore model (25,42,49,50). In a lipid bilayer in the liquid-disordered phase, various thermal motions of lipid molecules are observed. For example, lateral diffusion of a lipid, extensive conformational changes of hydrocarbon chains and hydrophilic segments, protrusion, and undulation motions of the membrane. Thermal fluctuation in the lipid density of lipid bilayers occurs, which transiently induces a nanodomain with smaller lipid density (i.e., a prepore) (51-53). The structure of the prepore is unstable because at the wall of the prepore the outer and the inner monolayers bend to connect with each other, producing extra free energy termed line tension. Thus, if such a prepore is formed, it immediately closes. However, if peptides are bound to the outer monolayer, a peptide can bind to the wall of a prepore immediately after it forms, which may

greatly decrease the line tension, and thereby decrease the free energy of the prepore. As a result, the prepore becomes stabilized, increasing its lifetime. During this brief existence, the peptide can diffuse laterally along the combined monolayer at the prepore, and then reach the inner monolayer (49). This lateral diffusion of the peptide at the wall of the prepore is enhanced by the electric field due to the membrane potential (25). This prepore model can explain the translocation of Rh-LfcinB (4-9) across the lipid bilayer and the increase in the rate of translocation with increasing negative membrane potential.

The results in this report indicate that the rate of entry of Rh-LfcinB (4-9) in septating cells was greater than that in non-septating cells. It is well recognized that Z-ring generates inward forces to make a septum formation (54-56). One can reasonably infer that this inward force stretches the cell membrane uniformly in the total area or locally near the septum region, depending on the interaction between peptidoglycan layer and the cell membrane. Recently, we demonstrated that the stretching of lipid bilayer increases the rate of entry of CPP TP10 into the single GUV lumen, which can be explained by the prepore model because the membrane tension induced by the stretching of the membrane increases the rate of prepore formation (50). As discussed in the previous paragraph, the translocation of Rh-LfcinB (4-9) across the lipid bilayer can be explained by the prepore model. Based on this model, the stretching of the cell membrane at the septum region is one of the main causes of the increase in the rate of entry of Rh-LfcinB (4-9) in septating cells.

Using the time-kill method we demonstrated that the presence of CCCP inhibits the antimicrobial activity of Rh-LfcinB (4-9) against *E. coli* cells, which correlates with the results using CLSM that Rh-LfcinB (4-9) does not enter their cytosol in the presence of CCCP. These results indicate that the antimicrobial activity of Rh-LfcinB (4-9) greatly decreases in the absence

of negative membrane potential because this peptide cannot enter the cytosol effectively. On the other hand, our results indicate that only 15 min exposure of 100 μM CCCP to *E. coli* cells decreases the cell viability by 23%, indicating that in most cells the effect of removal of membrane potential is reversible, i.e., the absence of membrane potential does not induce the cell death in *E. coli* cells although it suppresses the cell division (22), and after membrane potential is reproduced by removing CCCP the normal cell growth occurs. It was reported that *E. coli* cells can grow in the presence of CCCP (i.e., in the absence of proton motive force or membrane potential) at neutral and alkaline pH based on the results using the turbidity measurement (57,58). Later, it was demonstrated using the time-kill method that 5 h exposure of 100 μM CCCP to *E. coli* cells in a medium without glucose decreases the cell viability by 14%, but that in a medium containing 50 mM glucose decreases the cell viability by more than 99% (59). In our experiments, we used the EZ rich medium containing 11 mM glucose. Other factors instead of membrane potential (growth phase and acidic pH etc.) can explain the lethal effect of CCCP on *E. coli* cells (59).

Here, we compare the results of the interaction of Rh-LfcinB (4-9) with single *E. coli* cells in an EZ rich medium (obtained in this study) with those for single *E. coli* cells in a buffer (10 mM PIPES buffer, pH 7.0, 150 mM NaCl, 1 mM EGTA) (10). The greatest difference between the EZ rich medium and the buffer is the amount of nutrients, i.e., the buffer does not contain nutrients and thus the *E. coli* cells are under a starvation condition (30-33). The most important cell response under a starvation condition is a decrease or cessation of growth. We observed an increase in the cell length of a cell fixed on a poly-lysine coated cover slip in the EZ rich medium (8), whereas no increase in cell length was observed on the cover slip in the buffer (10). Another important difference is that *E. coli* cells in buffer can be strongly adsorbed on a coverslip (without poly-lysine coating), whereas those in the EZ rich medium cannot be adsorbed on a coverslip without

poly-lysine coating (i.e., a poly-lysine coating is necessary to fix cells on the coverslip). This is due to the starvation-induced decrease in cellular motility (31). The rate of entry of Rh-LfcinB (4-9) in the EZ rich medium is similar to that in the buffer. However, there is some difference in Rh-LfcinB (4-9)-induced leakage of calcein: at low concentrations (≤ 5 μM) no leakage occurred in either case, whereas a high concentration (9 μM) induced calcein leakage from some *E. coli* cells in the EZ rich medium but not from those in the buffer. The MIC of Rh-LfcinB (4-9) is 5 μM (10), and the effective concentration of peptide for single cell experiments is higher than that for the cell suspension method used in the MIC assay. Therefore, a very high concentration of peptide may induce leakage of calcein. Currently, the mechanism for the high concentration of Rh-LfcinB (4-9)-induced cell membrane damage of *E. coli* cells in the EZ rich medium (in contrast to the lack of cell membrane damage in cells in the buffer) has not been clarified. On the other hand, calcein photobleaching was not observed in *E. coli* cells in the buffer but occurred in *E. coli* cells in the EZ rich medium. This discrepancy may be explained by the oxygen concentration in the cytosol of *E. coli* cells. The oxygen concentration in the cytosol of *E. coli* cells in the EZ rich medium is high because these cells actively produce oxygen, whereas those in the buffer are not actively producing oxygen and hence the oxygen concentration in the cytosol is low. In the case of spheroplast, calcein photobleaching was observed. The spheroplast buffer used in the experiments of spheroplasts contained a high concentration of sucrose, which is an important nutrient. Thus, we can infer that the spheroplasts can produce oxygen gas and its concentration in the spheroplast cytosol is similar to that in the cytosol of *E. coli* cells.

The membrane potential plays various important roles in bacterial cell membranes. The activity of AMPs, such as cell membrane damage (8,24) and translocation across the cell membrane to enter the cytosol (this study), depends greatly on the membrane potential. During the

long evolution of AMPs in their interactions with bacterial cells, the structure of AMPs might have been modified to utilize the membrane potential to increase their interaction with bacterial cell membranes, improving their antimicrobial activity.

Conclusion

In this study, by simultaneously measuring the time courses of peptide entry (into the cytosol of *E. coli* cells and their spheroplasts, and the lumen of *E. coli* lipid-GUVs) and leakage of internal contents, we clearly revealed peptide entry without or before pore formation in the membrane. Using this method, we clearly showed that the membrane potential increases the rate of Rh-LfcinB (4-9) entry into the cytosol of *E. coli* cells and their spheroplasts, and the lumen of *E. coli* lipid-GUVs without pore formation. To the best of our knowledge, this is the first report demonstrating the role of the membrane potential in the antimicrobial activity of CPP-type AMPs and in their entry into the cytoplasm, which is a key process to determine their antimicrobial activity. These results indicate that the antimicrobial activity of Rh-LfcinB (4-9) and hence LfcinB (4-9) increases with increasing negative membrane potential.

Experimental procedures

Materials

E. coli polar lipid extract, DOPG, and DOPC were purchased from Avanti Polar Lipids, Inc. (Alabaster, AL, USA). Bovine serum albumin (BSA) and Nutrient Broth Medium containing Bacto peptone, beef extract, and agar were purchased from Fuji Film Wako Pure Chemical Co. (Osaka, Japan). Alexa Fluor 647 hydrazide (AF647), and calcein-acetoxymethyl (calcein-AM) were purchased from Invitrogen (Carlsbad, CA, USA). Cephalexin, poly-L-lysine,

deoxyribonuclease I (DNAase I), lysozyme, and CCCP were purchased from Sigma-Aldrich Co. (St. Louis, MO, USA). Lissamine rhodamine B Red (LRB Red) succinimidylester was purchased from AAT Bioquest Inc. (Sunnyvale, CA, USA). Tetraethylammonium chloride (TEAC) was purchased from Tokyo Chemical Industry Co., Ltd., Tokyo, Japan. EZ Rich Defined Medium (EZ rich medium) was purchased from TEKnova (Hollister, CA, USA).

LfcinB (4-9) was synthesized according to the FastMoc method using a 433A peptide synthesizer (PE Applied Biosystems, Foster City, CA, USA) and an Initiator+Alstra (Biotage, Uppsala, Sweden). RRWQWR has an amide-blocked C terminus. The fluorescence probe LRB red-labeled LfcinB (4-9) (Rh-LfcinB (4-9)), which has one fluorophore Rh at the N-terminus of the peptide, was synthesized using a reaction of LRB Red succinimidylester with LfcinB (4-9)-peptide resin (10). The methods for purification and identification using mass spectrometry of these peptides were described previously (10). Rh-LfcinB (4-9) concentrations in buffer were determined by absorbance using the molar extinction coefficient of Rh at 568 nm (i.e., 95,000 $M^{-1}cm^{-1}$).

Interaction of Rh-LfcinB (4-9) with single E. coli cells containing calcein

E. coli (JM-109) suspensions in EZ rich medium (containing 50 mM NaCl and 1.3 mM K_2HPO_4 as main ion sources (34)) were prepared according to the previously described method (8). The method of calcein loading to the cytosol of *E. coli* cells was as described previously (8,35). The *E. coli* suspension was transferred to a hand-made microchamber (60) with a poly-L-lysine coated coverslip (8).

Interactions of Rh-LfcinB (4-9) with single *E. coli* cells were observed using a confocal laser scanning microscope (FV-1000, Olympus, Tokyo, Japan). The microchamber was set on the thermoplate controlled at a temperature of 25 ± 1 °C (Thermoplate, Tokai Hit, Shizuoka, Japan)

(10). For CLSM measurements, fluorescence images of calcein (excited by 473 nm laser), Rh-LfcinB (4-9) (excited by 559 nm laser), and differential interference contrast (DIC) images were obtained using a 60× objective (10). During interaction of the peptide with single *E. coli* cells, Rh-LfcinB (4-9) in the medium was added continuously to the vicinity of single *E. coli* cells through a 20-μm-diameter glass micropipette, whose tip was located 50 μm from the target cell (8). The peptide solution was delivered through the micropipette by positive pressure (30 Pa). Details of these methods have been described previously (60,61).

To elucidate the effect of CCCP on the interaction of Rh-LfcinB (4-9) with single *E. coli* cells, a CCCP solution in EZ media containing DMSO was mixed with a suspension of *E. coli* cells containing calcein (final concentration of 100 μM CCCP, 0.5% DMSO, and 1×10^6 CFU/mL *E. coli* cells) and incubated for more than 10 min prior to interaction experiments (8).

Time-kill method to measure the antimicrobial activity of Rh-LfcinB (4-9)

An *E. coli* cell suspension in EZ rich medium (pH 7.3) was mixed with various concentrations of Rh-LfcinB (4-9) (final concentrations: $(3\sim10) \times 10^5$ CFU/mL and 2.0 or 5.0 μM peptide) in 5 mL microtube, and then the mixture was incubated in constant temperature incubator shaker (DWMax MBR-032P, TAITEC, Saitama, Japan) at 37 °C. At various time points of incubation, an aliquot was taken from the suspension and diluted with the medium, and then 40 μL of the resultant suspension was spread onto agar plates for CFU counting. After 24 h of incubation at 37 °C, we counted the number of bacterial colonies to obtain CFU/mL. Each measurement was performed three times using two replicates. Mean values of the fraction of viable cells and their standard deviations were obtained.

To investigate the effect of CCCP on the antimicrobial activity of Rh-LfcinB (4-9) against *E. coli* cells, we applied the time-kill method to examine the Rh-LfcinB (4-9)-induced decrease in

cell viability in the presence and absence of CCCP. An *E. coli* cell suspension in EZ rich medium was mixed with CCCP and after 5 min the mixture was mixed with Rh-LfcinB (4-9) (final concentrations: (2–3) × 10^6 CFU/mL, 100 μM CCCP and 5.0 μM peptide) in 5 mL microtube, and then the mixture was incubated at 25 °C for 15 min. At the same time, we prepared an *E. coli* cell suspension containing only 5.0 μM peptide (i.e., no CCCP) and that containing only 100 μM CCCP (i.e., no peptides) and incubated at 25 °C for 15 min as control experiments. An aliquot was then taken from each suspension and diluted 100 to 1000 times with the medium, and then 40 μL of the resultant suspension was spread onto agar plates for CFU counting. After 24 h of incubation at 37 °C, we counted the number of bacterial colonies to obtain CFU/mL. Each measurement was performed twice using two replicates. Mean values of the fraction of viable cells and their standard deviations were obtained.

Interaction of Rh-LfcinB (4-9) with single spheroplasts containing calcein

The method of preparing spheroplasts of *E. coli* cells was described previously (8, 62). The final buffer of the purified spheroplasts was 10 mM Tris-HCl (pH 7.8) containing 1.5 mM KCl, 48.5 mM NaCl, and 0.73 M sucrose (i.e., spheroplast buffer). The spheroplasts were used within 3 h of purification, without storing in the freezer. The method of calcein loading to the spheroplast cytosol was described previously (8).

The interaction of Rh-LfcinB (4-9) with single spheroplasts was investigated at 25 ± 1 °C using the same method described in the above section. In observing the interaction of Rh-LfcinB (4-9) with single spheroplasts for 10 min, we measured the FI due to calcein for 20–30 s (sometime 60 s) intermittently (every 50 s or 200 s) by closing the shutter of the 473 nm laser (for calcein) to prevent photobleaching of calcein (63), whereas we continuously measured the FI due to Rh-LfcinB (4-9).

To elucidate the effect of CCCP on the interaction of Rh-LfcinB (4-9) with single spheroplasts, a CCCP solution in the same buffer containing DMSO was mixed with the suspension of spheroplasts containing calcein (final concentration of 100 μM CCCP and 0.5% DMSO), and then incubated for more than 10 min prior to the interaction experiments.

Interactions of Rh-LfcinB (4-9) with single GUVs containing small GUVs

To detect the entry of Rh-LfcinB (4-9) into the GUV lumen, we used the single GUV method for CPPs (25,29). In this method, target GUVs (i.e., mother GUVs) contain small GUVs in the mother GUV lumen. For this purpose, we prepared *E. coli*-lipid-GUVs containing small DOPG/DOPC-GUVs in the mother GUV lumen (25,29). First, GUVs of DOPG/DOPC (1/1; molar ratio) membranes (i.e., DOPG/DOPC (1/1)-GUVs) were prepared in buffer C (10 mM PIPES, pH 7.0, 1 mM EGTA, 50 mM NaCl) containing 0.10 M sucrose using the natural swelling method. Briefly, DOPG and DOPC mixture in chloroform solution in glass vial was dried by nitrogen gas to prepare a thin lipid film and then the chloroform in the film was completely removed by a rotary vacuum pump (GCD-051X, ULVAC, Kanagawa, Japan) for more than 12 h to obtain a dry lipid film (24,64). It is very important to remove chloroform from the lipid films to prepare GUVs comprising oil-free membranes. If a GUV membrane contains small amounts of organic solvents such as chloroform, its physical properties change significantly (65) and membrane permeability of charged large molecules such as organic fluorescent probes (e.g., calcein) increases greatly (66,67). The dry lipid film was prehydrated with a small amount of Milli-Q, then incubated with buffer C at 37 °C for 1 h (24,64), and finally multilamellar vesicles and lipid aggregates were removed from the GUV suspension by centrifugation (10). The supernatant containing DOPG/DOPC-GUVs was mixed with AF647 solution in buffer C containing 0.10 M sucrose (final AF647 concentration of 6.0 μM). A dry lipid film of *E. coli* polar lipids was prepared using the

above method used for preparation of the dry DOPG/DOPC film. After prehydration, the lipid film of *E. coli* polar lipids was incubated with the DOPG/DOPC-GUV suspension containing AF647 in buffer C containing 0.10 M sucrose at 37 °C for 2 h (10). The resultant GUV suspension was purified using the membrane filtering method to remove untrapped fluorescent probes (64).

A purified suspension of GUVs containing small GUVs was transferred to a hand-made microchamber whose glass surface was coated with BSA (60,61). Interactions of Rh-LfcinB (4-9) with single GUVs were observed using a confocal laser scanning microscope (FV-1000, Olympus). The microchamber was set on the thermoplate controlled at a temperature of 25 ± 1 °C (Thermoplate, Tokai Hit) (10). For CLSM measurements, fluorescence images of Rh-LfcinB (4-9) (excited by 559 nm laser), AF647 (excited by 635 nm laser) and DIC images were obtained using a 60× objective (10). During the interaction of the peptide with single GUVs, the peptide in buffer C containing 0.1 M glucose was added continuously to the vicinity of the GUV using a 20-μm-diameter glass micropipette, whose tip was located 50 μm from the target GUV, by applying a positive pressure (30 Pa) inside the micropipette. Details of this experimental method and the analysis method to obtain the time course of the FI of GUVs were described in our previous papers (60,61).

Interactions of Rh-LfcinB (4-9) with single GUVs under membrane potential

To induce $\Delta\varphi$ in GUVs, we applied the method using a K^+ concentration gradient across the GUV membrane containing gramicidin A (8,24-26). Gramicidin A forms a dimer in lipid bilayers and acts as an ion channel for monovalent cations (68,69). For this purpose, we prepared GUVs of *E. coli*-lipid/ gramicidin A (molar ratio: 100/0.01) from a dry lipid film in buffer K (10 mM PIPES, pH 7.0, 50 mM KCl, 1 mM EGTA) containing 0.10 M sucrose, partially purified DOPG/DOPC (1/1)-GUVs prepared in the same buffer K containing 0.10 M sucrose, and 6.0 μM AF647 by the

natural swelling method, and purified them by the membrane filtering method. Then, we diluted the purified suspension with buffer T (10 mM PIPES, pH 7.0, 50 mM TEAC, 1 mM EGTA) containing 0.1 M glucose at various ratios. The membrane potential difference across a GUV membrane ($\Delta\varphi$) at 25 °C was calculated using the following equation:

$$\Delta\varphi = 25.7 \ln \frac{[K^+]_{out}}{[K^+]_{in}} (mV) \qquad (1)$$

where $[K^+]_{out}$ and $[K^+]_{in}$ are the K^+ concentration outside and inside the GUV, respectively. We waited for 10 min after application of the K^+ gradient to attain an equilibrium, and then we started the interaction experiment of Rh-LfcinB (4-9) with single GUVs with a membrane potential using the same method described in the previous section. For this purpose, Rh-LfcinB (4-9) solution was prepared using the same buffer as used outside the GUVs.

Acknowledgements: This work was supported in part by a Grant-in-Aid for Scientific Research (B) (No. 19H03193) from the Japan Society for the Promotion of Science (JSPS) to M.Y. This work was also supported in part by the Cooperative Research Project of the Research Center for Biomedical Engineering.

Conflict of interest: The authors declare that they have no conflicts of interest with the contents of the article.

Author contributions: FH and MY designed the experiments. FH and HD performed experiments. FH and MY analyzed the results. FH and MY wrote the paper.

REFERENCES

1. Hwang PM, Vogel HJ. 1998. Structure-function relationships of antimicrobial peptides. Biochem Cell Biol 76:235-246.

2. Zasloff M. 2002. Antimicrobial peptides of multicellular organisms. Nature 415:389-395.

3. Yeaman MR, Yount NY. 2003. Mechanisms of antimicrobial peptide action and resistance. Pharmaco Rev 55:27-55.

4. Hancock REW, Hans-Georg S. 2006. Antimicrobial and host-defense peptides as new anti-infective therapeutic strategies. Nat Biotech 24:1551-1557.

5. Melo MN, Ferre R, Castanho ARB. 2009. Antimicrobial peptides: linking partition, activity and high membrane-bound concentrations. Nat Rev Microbiol 8:1-5.

6. Matsuzaki K (ed), (2019) Antimicrobial Peptides: Basic for Clinical Application, Springer Nature.

7. Sochacki KA, Barns KJ, Bucki R, Weisshaar JC. 2011. Real-time attack on single *Escherichia coli* cells by the human antimicrobial peptide LL-37. Proc Natl Acad Sci USA. 108:E77-E81.

8. Hossain F, Moghal MMR, Islam MZ, Moniruzzaman M, Yamazaki M. 2019. Membrane potential is vital for rapid permeabilization of plasma membranes and lipid bilayers by the antimicrobial peptide lactoferricin B. J Biol Chem 294:10449-10462.

9. Park CB, Yi K-S, Matsuzaki K, Kim MS, Kim SC. 2000. Structure-activity analysis of buforin II, a histone H2A-derived antimicrobial peptide: The proline hinge is responsible for the cell-penetrating ability of buforin II. Proc Natl Acad Sci USA 97:8245-8250.

10. Moniruzzaman M, Islam MZ, Sharmin S, Dohra H, Yamazaki M 2017. Entry of a Six-Residue Antimicrobial Peptide Derived from Lactoferricin B into Single Vesicles and *Escherichia coli* Cells without Damaging their Membranes. Biochemistry 56:4419-4431.

11. Splith K, Neundorf I. 2011. Antimicrobial peptides with cell-penetrating peptide properties and vice versa. Eur Biophys J 40**:**387-397.

12. Bahnsen JS, Franzyk H, Sayers EJ, Jones AT, Nielsen HM. 2015. Cell-penetrating antimicrobial peptides – prospectives for targeting intracellular infections. Pharm Res 32**:**1546-1556.

13. Tomasinsig L, Skerlavaj B, Papo N, Giabbai B, Shai Y, Zanetti M. 2006. Mechanistic and functional studies of the interaction of a proline-rich antimicrobial peptide with mammalian cells. J Biol Chem, 281**:**383-391.

14. Lau YE, Rozek A, Scott MG, Goosney DL, Davidson DJ, Hancock REW. 2005. Interaction and cellular localization of the human host defense peptide LL-37 with lung epithelial cells. Infect Immun 73:583-591.

15. Catle M, Nazarian A, Yi SS, Tempst P. 1999. Lethal effects of apidaecin on *Escherichia coli* involve sequential molecular interactions with diverse targets. J Biol Chem 274:32555-32564.

16. Otvos LJr, Insug O, Rogers ME, Consolvo PJ, Condie BA, Lovas S, Bulet P, Blaszczyk-Thurin M 2000. Interaction between heat shock proteins and antimicrobial peptides. Biochemistry 39:14150-14159.

17. Brogden KA. 2005. Antimicrobial peptides: pore formers or metabolic inhibitors in bacteria? Nat Rev Microbiol 3:238-250.

18. Yeaman M. R, Bayer AS, Koo S-P, Foss W, Sullam PM. 1998. Platelet microbicidal proteins and neutrophil defensing disrupt the *Staphlococcus aureus* cytoplasmic membrane by distinct mechanism of action. J Clin Invest 101**:**178-187.

19. Wu M, Maier E, Benz R, Hancock REW. 1999. Mechanism of interaction of different classes of cationic antimicrobial peptides with planar bilayers and with the cytoplasmic membrane of *Escherichia coli*. Biochemistry 38:7235-7242.

20. Blackiston DJ, McLaughlin KA, Levin M. 2009. Bioelectric controls of cell proliferation. Cell Cycle 8:3527-3536.

21. Sunderacruz S, Levin M, Kaplan DL. 2009. Role of membrane potential in the regulation of cell proliferation and differentiation. Stem Cell Rev Rep 5:231-246.

22. Strahl H, Hamoen LW. 2010. Membrane potential is important for bacterial cell division. Proc Natl Acad Sci USA 107**:**12281-12286.

23. Zhou Y, Wong, C-O, Cho K-J, van der Hoeven D, Liang H, Thakur DP, Luo J, Babic M, Zinsmaier KE, Zhu MX, Hu H, Venkatachalam K, Hancock JF. 2015. Membrane potential modulates plasma membrane phospholipid dynamics and K-Ras signaling. Science 349:873-876.

24. Rashid MMO, Moghal MMR, Billah MM, Hasan M, Yamazaki M. 2020. Effect of membrane potential on pore formation by the antimicrobial peptide magainin 2 in lipid bilayers. BBA-Biomembranes 1862**:**183381.

25. Moghal MMR, Islam MZ, Hossain F, Saha SK, Yamazaki M. 2020. Role of Membrane Potential on Entry of Cell-Penetrating Peptide Transportan 10 into Single Vesicles. Biophys J 118:57-69.

26. Moghal MMR, Hossain F, Yamazaki M. 2020. Action of antimicrobial peptides and cell-penetrating peptides on membrane potential revealed by the single GUV method. Biophys Rev 12:339-348.

27. Tomita M, Takase M, Bellamy W, Shimamura S. 1994. A review: The active peptide of lactoferrin, Acta Paediatr J 36:585-591.

28. Schibli DJ, Epand RF, Vogel HJ, Epand RM. 2002. Tryptophan-rich antimicrobial peptides: comparative properties and membrane interactions. Biochem Cell Biol 80:667-677.

29. Islam MZ, Ariyama H, Alam JM, Yamazaki M. 2014. Entry of cell-penetrating peptide transportan 10 into a single vesicle by translocating across lipid membrane and its induced pores. Biochemistry 53:386-396.

30. Groat EG, Schultz JE, Zychlinsky E, Bockman A, Matin A. 1986. Starvation proteins in *Escherichia coli*: Kinetics of synthesis and role in starvation survival. J Bacteriol 168:486-493.

31. Wei X, Bauer WD. 1998. Starvation-induced changes in motility, chemotaxis, and flagellation of *Rhizobium meliloti*. Appl Environ Microbiol 64:1708-1714.

32. Mandel MJ, Silhavy TJ. 2005. Starvation for different nutrients in *Escherichia coli* results in differential modulation of RpoS levels and stability. J Bacteriol 187**:**434-442.

33. Biselli E, Schink SJ, Gerland U. 2020. Slower growth of *Escherichia coli* leads to longer survival in carbon starvation due to a decrease in the maintenance rate. Mol Syst Biol 16**:**e9478.

34. Neidhardt FC, Bloch PL, Smith DF. 1974. Culture medium for enterobacteria. J Bacteriol 119:736-747.

35. Dubey GP, Ben-Yehuda S. 2011. Intercellular nanotubes mediate bacterial communication. Cell 144: 590-600.

36. CLSI, Methods for determining bactericidal activity of antimicrobial agents. Approved guideline. CLSI document M26-A. Clinical and laboratory standards institute, USA, 1998.

37. Wei L, LaBouyer MA, Darling LEO, Elmore DE. 2016. Bacterial spheroplasts as a model for visualizing membrane translocation of antimicrobial peptides. Antimicrobial Agents Chemo 60:6350-6352.

38. Daniels CJ, Bole DG, Quay SC, Oxender DL. 1981. Role for membrane potential in the secretion of protein into the periplasm of *Escherichia coli*. Proc Natl Acad Sci USA 78:5396-5400.

39. Madani F, Lindberg S, Langel Ű, Futaki S, Gräslund A. 2011. Mechanisms of cellular uptake of cell-penetrating peptides. J. Biophysics 414729.

40. Koren E, Torchilin VP. 2012. Cell-penetrating peptides: breaking through to the other side. Trends Mol Med 18:385-393.

41. Lonhienne TGA, Sagulenko E, Webb RI, Kee K-C, Franke J, Devos DP, Nouwens A, Carroll BJ, Fuerst JA. 2010. Endocytosis-like protein uptake in the bacterium *Gemmata obscuriglobus*. Proc Natl Acad Sic USA 107:12883-12888.

42. Islam MZ, Sharmin S, Moniruzzaman M, Yamazaki M. 2018. Elementary Processes for the Entry of Cell-Penetrating Peptides into Lipid Bilayer Vesicles and Bacterial Cells. Appl Microbiol Biotechnol 102**:**3879-3892.

43. Mishra A, Gordon VD, Yang L, Coridan R, Wong GCL. 2008. HIV TAT forms pores in membranes by inducing saddle-spray curvature: potential role of bidentate hydrogen bonding. Angew Chem Int Ed 47:2986-2989.

44. Ciobanasu C, Siebrasse JP, Kubitscheck U. 2010. Cell-penetrating HIV1 TAT peptides can generate pores in model membranes. Biophys J 99:153-162.

45. Mishra A, Lai GH, Schmidt NW, Sun VZ, Rodriguez AR, Tong R, Tang L, Cheng J, Deming TJ, Kamei DT, Wong GCL. 2011. Translocation of HIV TAT peptide and analogues induced by multiplexed membrane and cytoskeletal interactions. Proc Natl Acad Sci USA 108:16883-16888.

46. Berlose J-P, Convert O, Derossi D, Brunissen A, Chassaing G. 1996. Conformational and associative behaviours of the third helix of antennapedia homeodomain in membrane-mimetic environments. Eur J Biochem 242:372-386.

47. Kawamoto S, Takasu M, Miyakawa T, Morikawa R, Oda T, Futaki S, Nagao H. 2011. Inverted micelles formation of cell-penetrating peptide studied by coarse-grained simulation: Importance of attractive force between cell-penetrating peptides and lipid head group. J Chem Phys 134:095103.
48. Swiecicki J-M, Bartsch A, Tailhades J, Di Pisa M, Heller B, Chassaing G, Mansuy C, Burlina F, Lavielle S. 2014. The efficacies of cell-penetrating peptides in accumulating in large unilamellar vesicles depend on their ability to form inverted micelles. ChemBioChem 15:884-891.
49. Sharmin S, Islam MZ, Karal MAS, Shibly SUA, Dohra H, Yamazaki M. 2016. Effects of lipid composition on the entry of cell-penetrating peptide oligoarginine into single vesicles. Biochemistry 55:4154-4165.
50. Islam MZ, Sharmin S, Levadnyy V, Shibly SUA, Yamazaki M. 2017. Effects of Mechanical Properties of Lipid Bilayers on Entry of Cell-Penetrating Peptides into Single Vesicles. Langmuir 33:2433-2443.
51. Evans E, Smith BA. 2011. Kinetics of hole nucleation in biomembrane rupture. New J Phys 13: 095010.
52. Levadny V, Tsuboi T, Belaya M, Yamazaki M. 2013. Rate Constant of Tension-Induced Pore Formation in Lipid Membranes. Langmuir 29:3848-3852.
53. Akimov SA, Volynsky PE, Galimzyanov TR, Kuzmin PI, Pavlov KV, Batishchev OV. 2017. Pore formation in lipid membrane I: Continuous reversible trajectory from intact bilayer through hydrophobic defect to transversal pore. Sci Rep 7:12152.
54. Bramhill D. 1997. Bacterial cell division. Annu Rev Cell Dev Biol 13:395-424.
55. Lan G, Wolgemuth CW, Sun SX. 2007. Z-ring force and cell shape during division in rod-like bacteria. Proc Natl Acad Sci USA 104:16110-16115.

56. Osawa M, Erickson HP. 2013. Liposome division by a simple bacterial division machinery. Proc Natl Acad Sci USA 110:11000-11004.

57. Kinoshita N, Unemoto T, Kobayashi H. 1984. Proton motive force is not obligatory for growth of *Escherichia coli.* J. Bacteriol. 160:1074-1077.

58. Mugikura S, Nishikawa M, Igarashi K, Kobayashi H. 1990. Maintenance of a neural cytoplasmic pH is not obligatory for growth of *Escherichia coli* and *Streptococcus faecalis* at an alkaline pH. J. Biochem. 108:86-91.

59. Nagata S. 1995. Lethal effect of carbonyl cyanide *m*-chlorophenylhydrazone on *Escherichia coli* and a halotolelrant *Brevibacterium* species. Microbios 81:73-83.

60. Yamazaki M. 2008. The single GUV method to reveal elementary processes of leakage of internal contents from liposomes induced by antimicrobial substances. Adv Planar Lipid Bilayers and Liposomes. 7:121-142.

61. Karal MAS, Alam JM, Takahashi T, Levadny V, Yamazaki M. 2015. Stretch-Activated Pore of Antimicrobial Peptide Magainin 2. Langmuir 31:3391-3401.

62. Martinac B, Buechner M, Delcour AH, Adler J, Kung C. 1987. Pressure-sensitive ion channel in *Escherichia coli*. Proc Natl Acad Sci USA 84:2297-2301.

63. Hasan M, Saha SK, Yamazaki M. 2018. Effect of membrane tension on transbilayer movement of lipids. J Chem Phys 148:245101.

64. Tamba Y, Terashima H, Yamazaki M. 2011. A membrane filtering method for the purification of giant unilamellar vesicles. Chem Phys Lipids 164:351-358.

65. Walde P, Cosentino K, Engel H, Stano P. 2010. Giant vesicles: preparations and applications. ChemBioChem 11:848-865.

66. Lin C-C, Bachmann M, Bachler S, Venkatesan K, Dittrich PS 2018. Tunable membrane potential reconstituted in giant vesicles promotes permeation of cationic peptides at nanomolar concentrations. ACS Appl Mater Interfaces 10:41909-41916.

67. Gehan P, Kulifaj S, Soule P, Bodin JB, Amoura M, Walrant A, Sagan S, Thiam AR, Ngo K, Vivier V, Cribier S, Rodriguez N. 2020. Penetratin translocation mechanism through asymmetric droplet interface bilayers. BBA-Biomembranes 1862:183415

68. Hille B. 1992. Ionic channels of excitable membranes. 2nd ed. Sinauer Association Inc. Massachusetts.

69. Andersen OS. 1983. Ion movement through gramicidin A channels: Interfacial polarization effects on single-channel current measurements. Biophys J 41:135-146.

TABLE 1 Effect of CCCP on the antimicrobial activity of Rh-LfcinB (4-9)

	Mean fraction of viable cells ± SD*
Interaction of 5.0 μM Rh-LfcinB (4-9) with *E. coli* cells in the presence of 100 μM CCCP	0.71 ± 0.04
Interaction of 5.0 μM Rh-LfcinB (4-9) with *E. coli* cells in the absence of CCCP	0.24 ± 0.05
Interaction of no peptides with *E. coli* cells in the presence of 100 μM CCCP	0.77 ± 0.03

*Cell viability was measured after the interaction of peptides (or no peptides) with *E. coli* cells in the presence or the absence of CCCP at 25 °C for 15 min. Mean values of the fraction of viable cells and their standard deviations are shown.

Figure legends

Figure 1: Interaction of Rh-LfcinB (4-9) with single *E. coli* cells containing calcein. (A) CLSM images due to (1) calcein, (2) Rh-LfcinB (4-9), and (3) differential interference contrast (DIC) of an *E. coli* cell interacting with 5.0 μM Rh-LfcinB (4-9). The numbers above each image indicate the interaction time of peptides with the cell. The bar represents 2 μm. (B) The FI profiles along a white line in the cell shown in (A). Green line and red line correspond to the FI of calcein and Rh-LfcinB (4-9), respectively. To obtain each line profile, the FI profiles in the line of 3 consecutive images of the cell obtained by CLSM were superimposed to increase S/N. (C) Time course of change in the FI of the cell shown in (A). Green line and red line correspond to the FI of the cell due to calcein and that due to Rh-LfcinB (4-9), respectively. (D) Other examples of time course of the change in FI due to Rh-LfcinB (4-9) for several "single cells" under the same conditions as in (A). The curves labeled by "S" are for the septating cells and the nonlabeled curves are for the non-septating cells. (E) Dependence of P_{entry} (10 min) and P_{leak} (10 min) on peptide concentration. (red ■) P_{entry} (10 min) and (black ▲) P_{leak} (10 min).

Figure 2: Time-kill kinetics of Rh-LfcinB (4-9) against *E. coli* cells. (green ■) 5.0 μM and (red ▲) 2.0 μM Rh-LfcinB (4-9). (●) in the absence of the peptide. Mean values of the fraction of viable cells and their standard deviations are shown.

Figure 3: Interaction of Rh-LfcinB (4-9) with single *E. coli* cells comprising of calcein in presence of CCCP. (A) showing images from CLSM of (1) calcein, (2) Rh-LfcinB (4-9) and (3) DIC image on the interaction of *E. coli* with 5.0 μM Rh-LfcinB (4-9). The numbers top on each image showing the time in sec during the interaction of Rh-LfcinB (4-9) with *E. coli*. The bar is 2 μm. (B) Time course of FI change of the *E. coli* due to calcein (green line) and Rh-LfcinB (4-9) (red line).

Figure 4: Interaction of Rh-LfcinB (4-9) with single *E. coli*-spheroplasts containing calcein. (A) CLSM images due to (1) calcein, (2) Rh-LfcinB (4-9), and (3) DIC of a spheroplast interacting with 2.0 μM Rh-LfcinB (4-9). The numbers above each image indicate the interaction time of Rh-LfcinB (4-9) with the spheroplast. The bar represents 5 μm. (B) Time course of change in the FI of the spheroplast shown in (A) over time. Green line and red line correspond to the FI of the total spheroplast due to calcein and that due to Rh-LfcinB (4-9), respectively. Brown squares correspond to the rim intensity due to Rh-LfcinB (4-9). Blue triangles correspond to the FI of the central region of spheroplast due to Rh-LfcinB (4-9) determined by the following line profile analysis. (C) the FI profile along white line in the Rh- LfcinB (4-9) images at 0 s in the panel A(2). (D) Dependence of P_{entry} (10 min) on peptide concentration.

Figure 5: Interaction of Rh-LfcinB (4-9) with single *E. coli*-spheroplasts comprising of calcein. (A) showing images from CLSM of (1) calcein, (2) Rh-LfcinB (4-9) and (3) DIC image on the interaction of spheroplast with 3.0 μM Rh-LfcinB (4-9). The numbers top on each image showing the time in sec during the interaction. The bar is 5 μm. (B) Time course of FI change of total spheroplast due to calcein (green line) and Rh-LfcinB (4-9) (red line), spheroplast rim due to Rh-LfcinB (4-9) (brown square) and central region of spheroplast due to Rh-LfcinB (4-9) (blue triangles) (C) FI profile along white line in the Rh--LfcinB (4-9) images at 0 s in the panel A (2). (D) Dependence of P_{leak} (10 min) on peptide concentration.

Figure 6: Effect of CCCP on the interaction of Rh-LfcinB (4-9) with single *E. coli*-spheroplasts containing calcein. The final CCCP concentration was 100 μM. (A) CLSM images due to (1) calcein, (2) Rh-LfcinB (4-9), and (3) DIC of a spheroplast interacting with 5.0 μM Rh-LfcinB (4-9). The numbers above each image indicate the interaction time of Rh-LfcinB (4-9) with the spheroplast. The bar is 5 μm. (B) Time

course of change in the FI of the spheroplast shown in (A) over time. Green line and red line correspond to the FI of the spheroplast due to calcein and that due to Rh-LfcinB (4-9), respectively.

Figure 7: Interaction of Rh-LfcinB (4-9) with single *E. coli*-lipid-GUVs containing small GUVs. (A) CLSM images due to (1) AF647, (2) Rh-LfcinB (4-9), and (3) DIC of an *E. coli*-lipid-GUV interacting with 5.0 μM Rh-LfcinB (4-9) in the absence of membrane potential. The numbers above each image indicate the interaction time of Rh-LfcinB (4-9) with the GUV. The bar is 30 μm. (B) Time course of change in the FI of the GUV shown in (A) over time. Red squares and green triangles correspond to the FI of the GUV lumen due to AF647 and that of the GUV rim due to Rh-LfcinB (4-9), respectively. (C) Dependence of P_{entry} (10 min) on peptide concentration. (D) Time course of change in the rim intensity. Red circles and green triangles correspond to the rim intensity due to Rh-LfcinB (4-9) in the presence of 0.5 and 5.0 μM Rh-LfcinB (4-9), respectively.

Figure 8: Effect of $\Delta\varphi$ on the entry of Rh-LfcinB (4-9) into single *E. coli*-lipid-GUVs containing small GUVs. (A) (B) CLSM images due to (1) AF647, (2) Rh-LfcinB (4-9), and (3) DIC of an *E. coli*-lipid-GUV interacting with 0.50 μM Rh-LfcinB (4-9) under $\Delta\varphi = -102$ mV (A) and 0 mV (B). The numbers above each image indicate the interaction time of peptides with the GUV. The bar is 30 μm. (C) Time course of change in the FI of the GUV shown in (A) over time. Red squares and green triangles correspond to the FI of the GUV lumen due to AF647 and that of the GUV rim due to Rh-LfcinB (4-9), respectively. (D) Time course of change in the rim intensity. Red circles and green triangles correspond to the rim intensity due to Rh-LfcinB (4-9) in the presence of $\Delta\varphi = 0$ mV and −102 mV, respectively. (E) Effect of $\Delta\varphi$ on P_{entry} (10 min). (red ▲) 2.0 μM, (blue ●) 0.50 μM, and (■) 0.20 μM Rh-LfcinB (4-9).

Figure 1

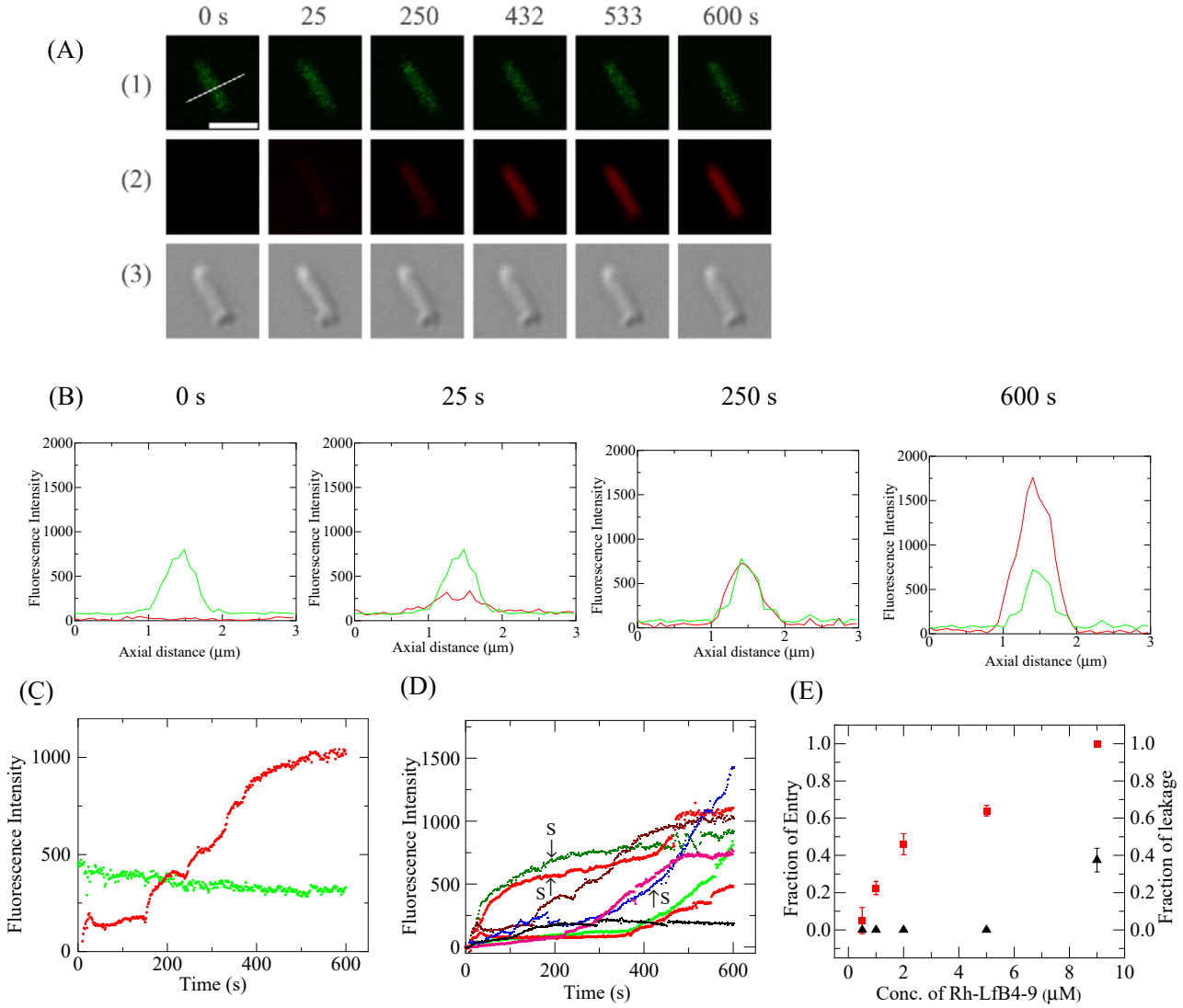

Figure 1: Interaction of Rh-LfcinB (4-9) with single *E. coli* cells containing calcein. (A) CLSM images due to (1) calcein, (2) Rh-LfcinB (4-9), and (3) differential interference contrast (DIC) of an *E. coli* cell interacting with 5.0 μM Rh-LfcinB (4-9). The numbers above each image indicate the interaction time of peptides with the cell. The bar represents 2 μm. (B) The FI profiles along a white line in the cell shown in (A). Green line and red line correspond to the FI of calcein and Rh-LfcinB (4-9), respectively. To obtain each line profile, the FI profiles in the line of 3 consecutive images of the cell obtained by CLSM were superimposed to increase S/N. (C) Time course of change in the FI of the cell shown in (A). Green line and red line correspond to the FI of the cell due to calcein and that due to Rh-LfcinB (4-9), respectively. (D) Other examples of time course of the change in FI due to Rh-LfcinB (4-9) for several "single cells" under the same conditions as in (A). The curves labeled by "S" are for the septating cells and the nonlabeled curves are for the non-septating cells. (E) Dependence of P_{entry} (10 min) and P_{leak} (10 min) on peptide concentration. (red ■) P_{entry} (10 min) and (black ▲) P_{leak} (10 min).

Figure 2

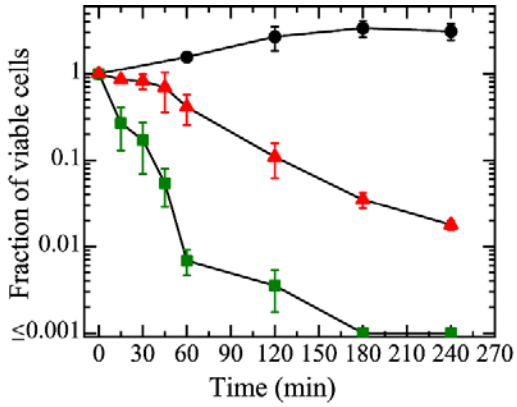

Figure 2: Time-kill kinetics of Rh-LfcinB (4-9) against *E. coli* cells. (green ■) 5.0 µM and (red ▲) 2.0 µM Rh-LfcinB (4-9). (●) in the absence of the peptide. Mean values of the fraction of viable cells and their standard deviations are shown.

Figure 3

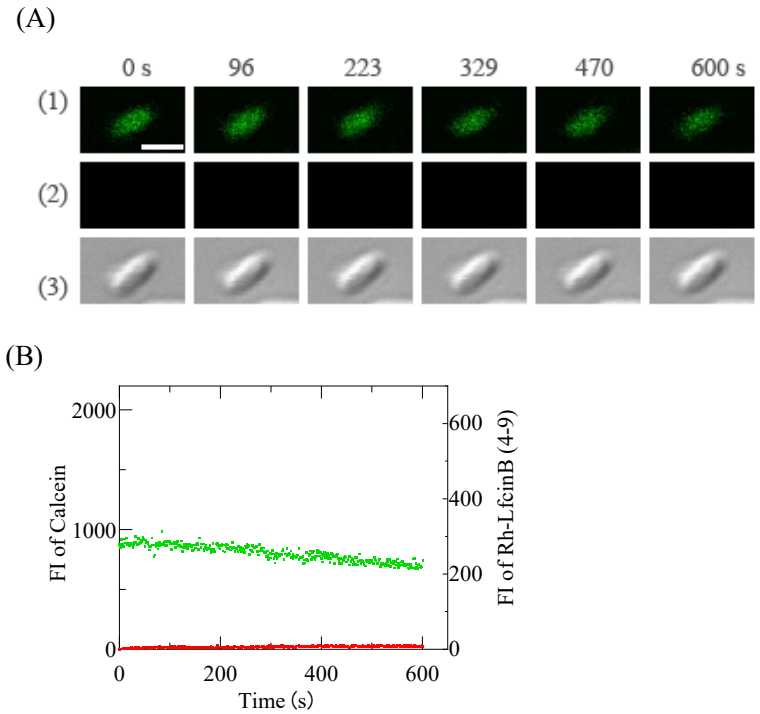

Figure 3: Interaction of Rh-LfcinB (4-9) with single *E. coli* cells comprising of calcein in presence of CCCP. (A) showing images from CLSM of (1) calcein, (2) Rh-LfcinB (4-9) and (3) DIC image on the interaction of *E. coli* with 5.0 µM Rh-LfcinB (4-9). The numbers top on each image showing the time in sec during the interaction of Rh-LfcinB (4-9) with *E. coli*. The bar is 2 µm. (B) Time course of FI change of the *E. coli* due to calcein (green line) and Rh-LfcinB (4-9) (red line).

Figure 4

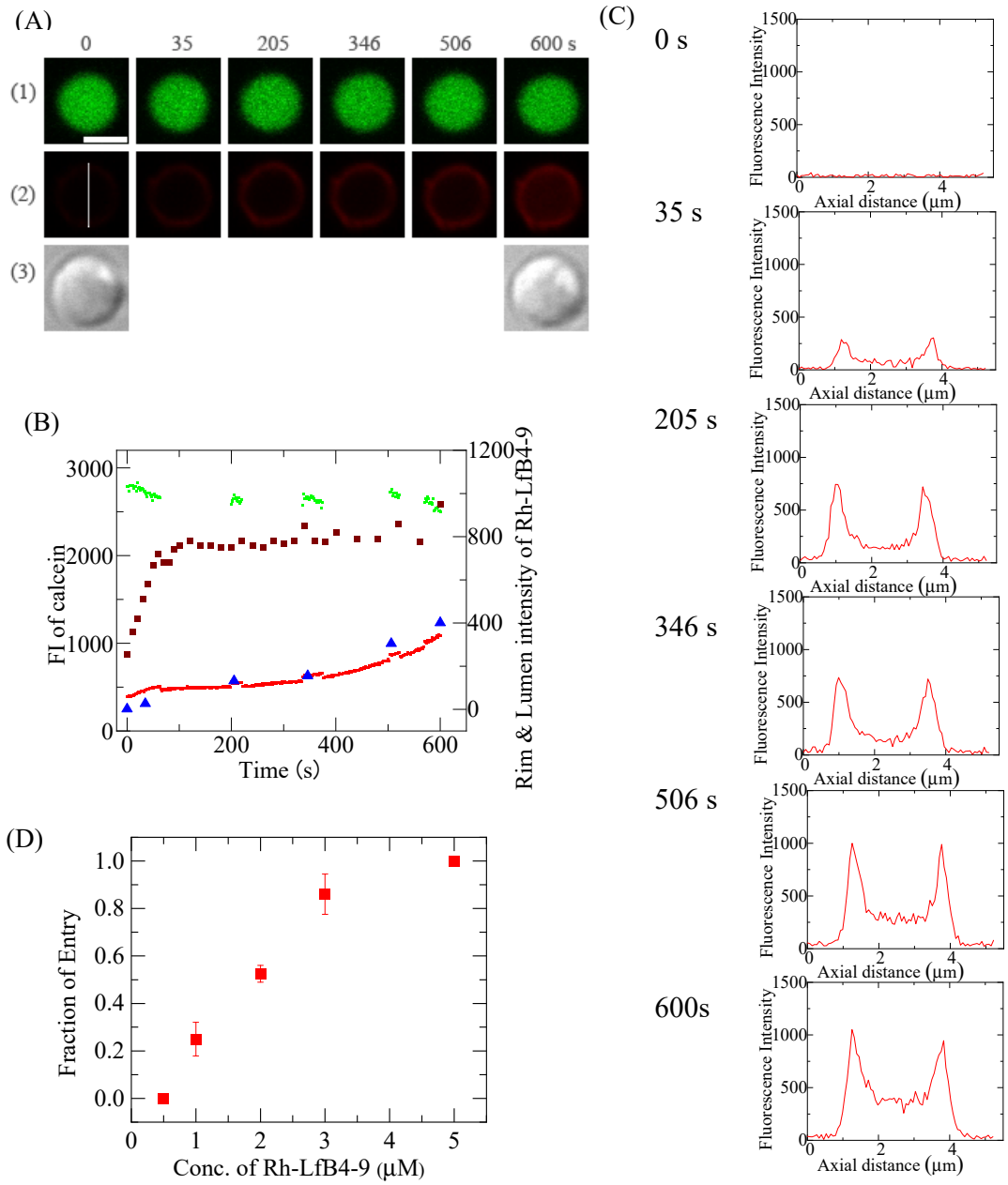

Figure 4: Interaction of Rh-LfcinB (4-9) with single *E. coli*-spheroplasts containing calcein. (A) CLSM images due to (1) calcein, (2) Rh-LfcinB (4-9), and (3) DIC of a spheroplast interacting with 2.0 μM Rh-LfcinB (4-9). The numbers above each image indicate the interaction time of Rh-LfcinB (4-9) with the spheroplast. The bar represents 5 μm. (B) Time course of change in the FI of the spheroplast shown in (A) over time. Green line and red line correspond to the FI of the total spheroplast due to calcein and that due to Rh-LfcinB (4-9), respectively. Brown squares correspond to the rim intensity due to Rh-LfcinB (4-9). Blue triangles correspond to the FI of the central region of spheroplast due to Rh-LfcinB (4-9) determined by the following line profile analysis. (C) the FI profile along white line in the Rh- LfcinB (4-9) images at 0 s in the panel A(2). (D) Dependence of P_{entry} (10 min) on peptide concentration.

Figure 5

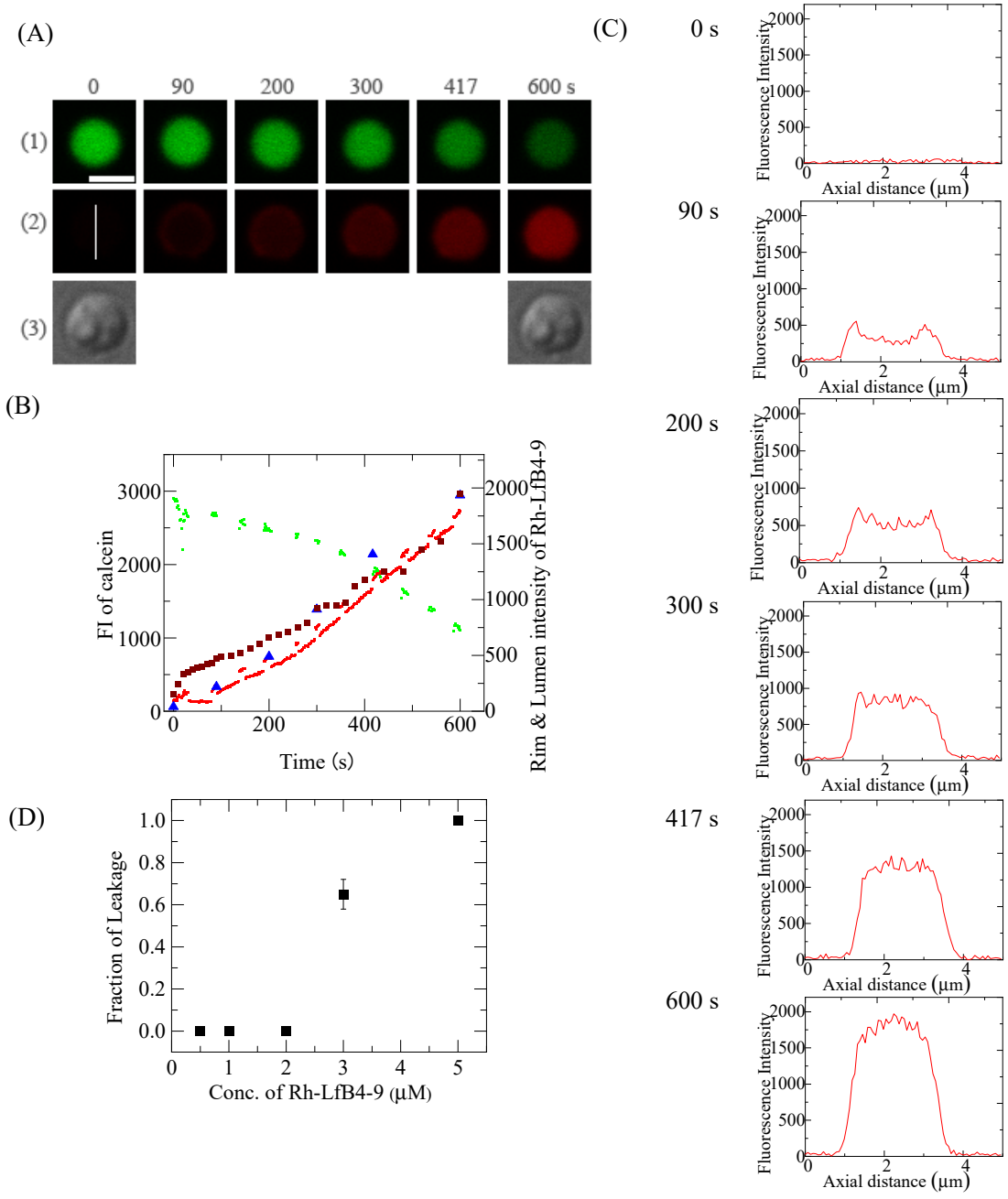

Figure 5: Interaction of Rh-LfcinB (4-9) with single *E. coli*-spheroplasts comprising of calcein. (A) showing images from CLSM of (1) calcein, (2) Rh-LfcinB (4-9) and (3) DIC image on the interaction of spheroplast with 3.0 μM Rh-LfcinB (4-9). The numbers top on each image showing the time in sec during the interaction. The bar is 5 μm. (B) Time course of FI change of total spheroplast due to calcein (green line) and Rh-LfcinB (4-9) (red line), spheroplast rim due to Rh-LfcinB (4-9) (brown square) and central region of spheroplast due to Rh-LfcinB (4-9) (blue triangles) (C) FI profile along white line in the Rh--LfcinB (4-9) images at 0 s in the panel A (2). (D) Dependence of P_{leak} (10 min) on peptide concentration.

Figure 6

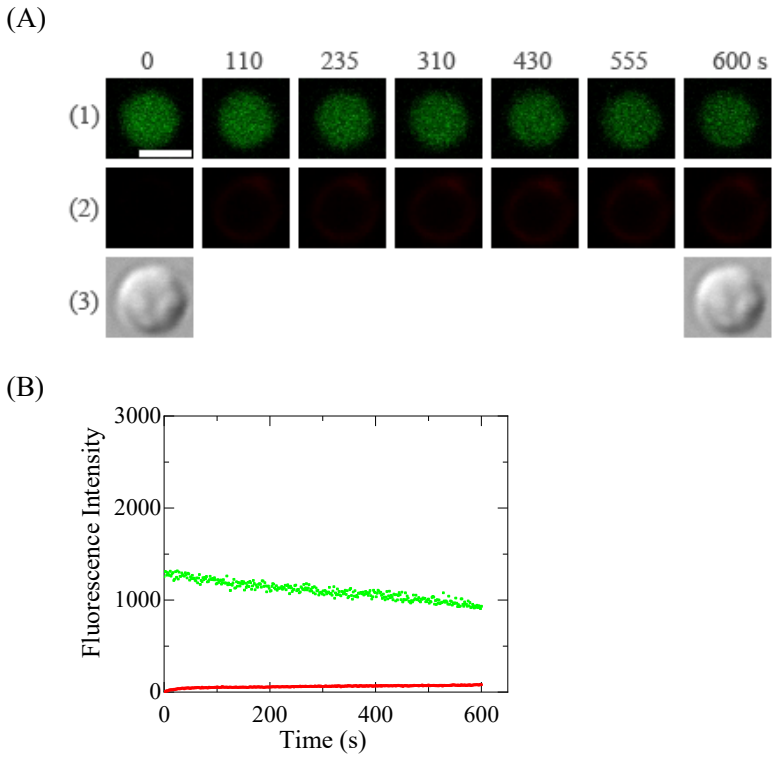

Figure 6: Effect of CCCP on the interaction of Rh-LfcinB (4-9) with single *E. coli*-spheroplasts containing calcein. The final CCCP concentration was 100 µM. (A) CLSM images due to (1) calcein, (2) Rh-LfcinB (4-9), and (3) DIC of a spheroplast interacting with 5.0 µM Rh-LfcinB (4-9). The numbers above each image indicate the interaction time of Rh-LfcinB (4-9) with the spheroplast. The bar is 5 µm. (B) Time course of change in the FI of the spheroplast shown in (A) over time. Green line and red line correspond to the FI of the spheroplast due to calcein and that due to Rh-LfcinB (4-9), respectively.

Figure 7

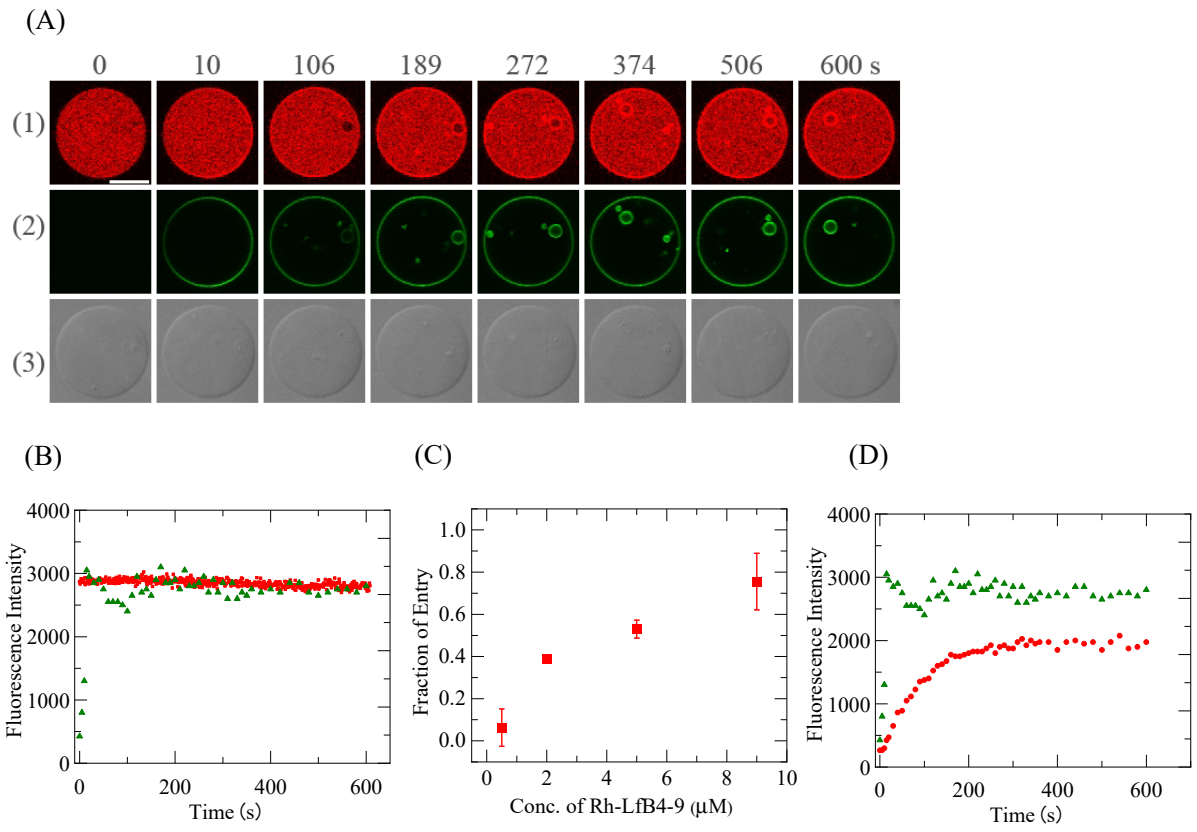

Figure 7: Interaction of Rh-LfcinB (4-9) with single *E. coli*-lipid-GUVs containing small GUVs. (A) CLSM images due to (1) AF647, (2) Rh-LfcinB (4-9), and (3) DIC of an *E. coli*-lipid-GUV interacting with 5.0 μM Rh-LfcinB (4-9) in the absence of membrane potential. The numbers above each image indicate the interaction time of Rh-LfcinB (4-9) with the GUV. The bar is 30 μm. (B) Time course of change in the FI of the GUV shown in (A) over time. Red squares and green triangles correspond to the FI of the GUV lumen due to AF647 and that of the GUV rim due to Rh-LfcinB (4-9), respectively. (C) Dependence of P_{entry} (10 min) on peptide concentration. (D) Time course of change in the rim intensity. Red circles and green triangles correspond to the rim intensity due to Rh-LfcinB (4-9) in the presence of 0.5 and 5.0 μM Rh-LfcinB (4-9), respectively.

Figure 8

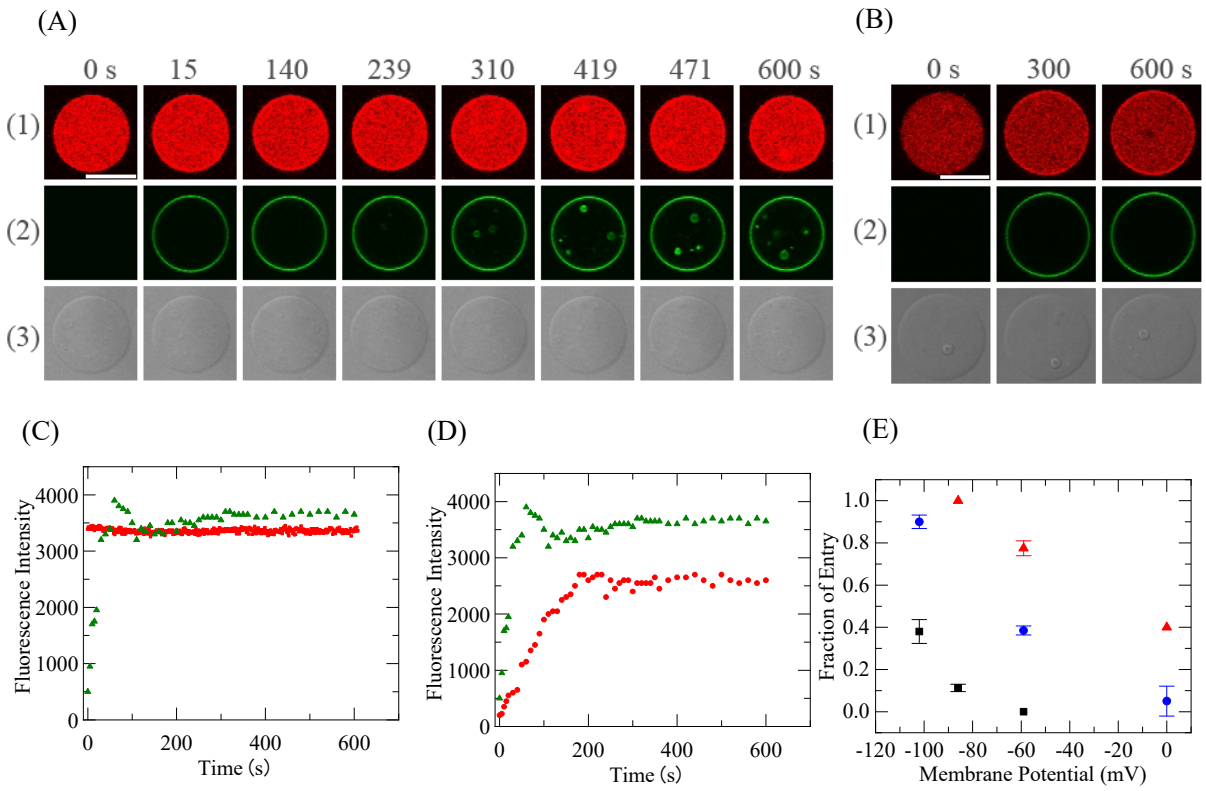

Figure 8: Effect of $\Delta\varphi$ on the entry of Rh-LfcinB (4-9) into single *E. coli*-lipid-GUVs containing small GUVs. (A) (B) CLSM images due to (1) AF647, (2) Rh-LfcinB (4-9), and (3) DIC of an *E. coli*-lipid-GUV interacting with 0.50 μM Rh-LfcinB (4-9) under $\Delta\varphi = -102$ mV (A) and 0 mV (B). The numbers above each image indicate the interaction time of peptides with the GUV. The bar is 30 μm. (C) Time course of change in the FI of the GUV shown in (A) over time. Red squares and green triangles correspond to the FI of the GUV lumen due to AF647 and that of the GUV rim due to Rh-LfcinB (4-9), respectively. (D) Time course of change in the rim intensity. Red circles and green triangles correspond to the rim intensity due to Rh-LfcinB (4-9) in the presence of $\Delta\varphi = 0$ mV and −102 mV, respectively. (E) Effect of $\Delta\varphi$ on P_{entry} (10 min). (red ▲) 2.0 μM, (blue ●) 0.50 μM, and (■) 0.20 μM Rh-LfcinB (4-9).